

1 **The Influences of Mass Loading and Rapid Dilution of**
2 **Secondary Organic Aerosol on Particle Volatility**

3

4 **Katheryn R. Kolesar¹, Claudia Chen^{1,*}, David Johnson^{1,%} and Christopher D. Cappa¹**

5 [1] Department of Civil and Environmental Engineering, University of California, Davis, One
6 Shields Avenue, Davis, California 95616, United States

7 [*] now at: Sustainable Energy Initiative, Santa Clara University, 500 El Camino Real, Santa
8 Clara, California 95053 United States

9 [%] now at: Advanced Light Source, Lawrence Berkeley National Laboratory, 1 Cyclotron Rd,
10 Berkeley, California 94720, United States

11 Correspondence to: C.D. Cappa (cdcappa@ucdavis.edu)

12

1 **Abstract**

2 The thermally-induced evaporation of secondary organic aerosol (SOA) has been characterized
3 for SOA formed from the dark ozonolysis of α -pinene + O_3 at initial mass concentrations ranging
4 from 1 to $800 \mu\text{g m}^{-3}$. Temperature-dependent particle size distributions were measured using a
5 thermodenuder and the resulting mass thermograms were compared between the SOA formed at
6 the various SOA mass concentrations. Negligible differences were observed between the mass
7 thermograms for SOA concentrations $< 300 \mu\text{g m}^{-3}$. At higher SOA concentrations, the observed
8 mass thermograms indicated the SOA was actually slightly less volatile than the SOA at lower
9 concentrations; this is likely an artifact due to either saturation of the gas-phase or to
10 re-condensation during cooling. The thermograms observed when the SOA was formed at high
11 concentrations ($>380 \mu\text{g m}^{-3}$) and then rapidly isothermally diluted to low concentrations ($1\text{-}20 \mu\text{g}$
12 m^{-3}) were identical to those for the SOA that was initially formed at low concentrations. The
13 experimental results were compared to a kinetic model that simulates particle evaporation upon
14 heating in a thermodenuder for a given input volatility distribution and particle composition. Three
15 cases were considered: 1) the SOA was composed of semi-volatile monomer species with a
16 volatility distribution based on that derived previously from consideration of SOA growth
17 experiments; 2) the initial SOA was composed almost entirely of non-volatile dimers that
18 decompose upon heating into their semi-volatile monomer units, which can then evaporate; and 3)
19 where a volatility distribution was derived by fitting the model to the observed mass thermograms.
20 It was found that good agreement is obtained between model predictions and the observations
21 when the particle composition is either dominated by compounds of low volatility or by dimers.
22 These same models were used to simulate isothermal evaporation of the SOA and were found to
23 be broadly consistent with literature observations that indicate that SOA evaporation occurs with
24 multiple timescales. The use of the semi-volatile monomer volatility distribution fails to reproduce
25 the observed evaporation. The presence of dimers and larger oligomers in secondary organic
26 aerosol formed from products of the reaction of α -pinene and O_3 has been well-established in
27 laboratory studies. However, the timescale and relative importance of the formation of oligomers
28 or low volatility compounds in the growth and evaporation of SOA has been debated. This study
29 provides further support that low volatility compounds and oligomers are formed in α -pinene + O_3
30 in high abundances and suggests that their formation occurs rapidly upon particle formation.

1 1 Introduction

2 Atmospheric aerosol particles have an important impact on human health (Chen et al., 2013)
3 and climate (IPCC, 2014). Organic aerosol (OA) is a significant portion of atmospheric particulate
4 mass, often contributing 20-90% of the fine particle mass world-wide (Saxena and Hildemann,
5 1996;Andreae and Crutzen, 1997), a major portion of which is secondary organic aerosol (SOA)
6 (Zhang et al., 2005). One pathway through which SOA is formed is when products from the gas-
7 phase oxidation of volatile organic compounds (VOCs) condense onto pre-existing particles or
8 nucleate to form new particles. VOCs are broadly classified as being either biogenic (BVOCs) or
9 anthropogenic (AVOCs). The source of SOA varies with geographical location, with larger
10 contributions of anthropogenic SOA in and around urban areas (Weber et al., 2007) and larger
11 contributions of biogenic SOA in rural areas (Han et al., 2014).

12 An important source of biogenic SOA is the reaction of unsaturated gas-phase VOCs with O₃.
13 The most globally abundant BVOC compounds are isoprene (C₅H₈) and monoterpenes (C₁₀H₁₆)
14 (Kesselmeier and Staudt, 1999). Around 90 Tg C yr⁻¹ of monoterpenes are emitted from vegetation
15 sources worldwide (Hallquist et al., 2009) of which α -pinene constitutes nearly half (Guenther et
16 al., 1995;Seinfeld and Pankow, 2003). During the formation of SOA from the ozonolysis of α -
17 pinene the aerosol composition and corresponding physical properties have been shown to change
18 as a function of total organic aerosol mass loading (C_{OA}). For example, Shilling et al. (2009)
19 observe that both the O/C ratio and the effective density of α -pinene SOA decrease as C_{OA}
20 increases, most steeply below ~30 $\mu\text{g m}^{-3}$. Other studies have shown that the mass yield of a variety
21 of SOA, including α -pinene + O₃ SOA, increases as C_{OA} increases (Henry et al., 2012;Odum et
22 al., 1996;Pathak et al., 2007). Changes to aerosol composition as a function of C_{OA} can be
23 explained by gas/particle partitioning in which the distribution of material between the gas and
24 particle phases is related to the saturation vapor concentration, C^{*}, and the total OA concentration
25 (Pankow, 1994;Odum et al., 1996) according to:

26

$$27 \quad \frac{c_{i,p}}{c_{i,tot}} = \alpha_i \left(1 + \frac{c_i^*}{c_{OA}} \right)^{-1} \quad (1)$$

28

1 where $C_{i,p}$ is the concentration of compound i in the particle phase ($\mu\text{g m}^{-3}$), $C_{i,\text{tot}}$ is the total
2 concentration of i in both the gas and particle phase ($\mu\text{g m}^{-3}$), C_i^* is the saturation vapor
3 concentration ($\mu\text{g m}^{-3}$) and α_i is the mass yield of compound i . When C_{OA} is equal to C_i^* 50% of
4 compound i exists in the particle phase. Compounds are generally considered semi-volatile when
5 their C_i^* are within 1-2 orders of magnitude of the concurrent C_{OA} . According to gas/particle
6 partitioning, as C_{OA} increases the fraction of higher volatility compounds, which usually have a
7 lower O/C ratio, present in the condensed phase will increase. SOA growth experiments have
8 historically been interpreted through the framework of absorptive gas/particle partitioning theory,
9 where volatility distributions, i.e. distributions of α_i as a function of C_i^* for some number of
10 surrogate compounds, are derived by fitting the observed SOA formation (Odum et al.,
11 1996;Donahue et al., 2006). Such analyses indicate that SOA is composed of a distribution of
12 semi-volatile compounds with volatilities greater than $\sim 10^{-1} \mu\text{g m}^{-3}$. However, the volatility
13 distributions determined from fitting of growth experiments have been mostly unable to describe
14 the reverse process, namely evaporation of SOA. .

15 For example, quantitative estimates of the volatility of both ambient and laboratory OA after
16 heating induced evaporation indicate that there are often components of OA with significantly
17 lower volatility than predicted by fitting of growth experiments (Cappa and Jimenez, 2010;Stanier
18 et al., 2007). In addition, several experiments have observed slower than expected room-
19 temperature evaporation of both ambient (Vaden et al., 2011) and laboratory generated (Saleh et
20 al., 2013;Grieshop et al., 2007;Wilson et al., 2015;Vaden et al., 2011), SOA during isothermal
21 dilution. It has also been observed that the mass spectrum of α -pinene + O_3 SOA over the range
22 40-200 amu exhibited negligible changes during the heating induced evaporation (Cappa and
23 Wilson, 2011), even though absorptive gas/particle partitioning suggests an SOA composed of
24 components having volatilities spanning several decades of C^* . Some other experiments have
25 observed some changes to the observed particle composition (i.e. mass spectrum) upon heating
26 (Hall and Johnston, 2012b;Kostenidou et al., 2009), but overall the changes tend to be small and
27 inconsistent with the particles being composed of individual compounds with a wide range of
28 volatilities. Altogether these observations illustrate that there is a clear gap between the apparent
29 volatility of SOA as characterized during evaporation experiments and the effective volatility of
30 SOA derived from formation studies.

1 In this study, the volatility of α -pinene + O₃ SOA was characterized by heating-induced
2 evaporation in a thermodenuder (TD) as a function of C_{OA} over the range 1 to 800 $\mu\text{g m}^{-3}$. Based
3 on previous SOA formation experiments, the SOA composition is expected to have changed as
4 C_{OA} was increased from 1 $\mu\text{g m}^{-3}$ to >140 $\mu\text{g m}^{-3}$ (Shilling et al., 2009). It follows that the SOA
5 volatility should vary as a function of C_{OA} as well, with an expectation that SOA at higher C_{OA}
6 should be more volatile than that at low C_{OA} and thus should exhibit different responses to heating.
7 Additionally, mass thermograms of SOA that was initially formed at C_{OA} >380 $\mu\text{g m}^{-3}$ and rapidly
8 diluted to C_{OA} < 30 $\mu\text{g m}^{-3}$ were measured. The experimental results are interpreted using the
9 kinetic model of aerosol evaporation in a TD by Cappa (2010) that has been extended from the
10 original formulation that assumed direct evaporation of semi- or low-volatility monomers to
11 include dimer formation and decomposition. Good agreement between the experimental
12 observations and the model predictions provide support for the large influence of oligomer
13 decomposition on SOA evaporation.

14

15 **2 Materials and Methods**

16 **2.1 Secondary Organic Aerosol Production**

17 SOA was formed in the absence of seed particles at various total C_{OA} from the formation and
18 subsequent growth of nano-condensation nuclei that were formed from products of the ozonolysis
19 of gas-phase α -pinene, in excess (Fig. S1). Variable amounts of α -pinene were introduced into a
20 stainless steel flowtube (L = 2 m; ID = 2.3 cm) by constantly injecting liquid α -pinene (0.12-0.7
21 $\mu\text{L h}^{-1}$) into a stream of purified house air at 0.015 lpm. The O₃ was generated by passing air
22 through a cell containing a 22.9 cm long Hg pen-ray lamp (UVP, LLC.) and then 0.70-1.0 lpm of
23 this flow was sub-sampled into the flowtube. The relative humidity of the air stream was ~30%
24 for all experiments. The concentrations of α -pinene, O₃ and other experiment-specific conditions
25 are given in Table 1. The residence time in the flow tube was typically about 1 minute, although
26 slightly variable depending on the total volumetric flow rate (see Table 1). No OH scavenger was
27 used. The O₃ concentration was measured using an O₃ Monitor (Model 450, API Inc.).
28 Downstream of the flowtube residual hydrocarbons and O₃ were removed by passing the airstream
29 through a Carulite 200 (Carus) catalyst and a charcoal denuder. The particles were assumed to
30 have a density of 1.2 $\mu\text{g m}^{-3}$. The particle mass concentrations were varied from 1 to 800 $\mu\text{g m}^{-3}$

1 although were kept stable for the duration of each experiment. Larger concentrations tended to
2 correspond to particle size distributions that peaked at larger sizes.

3 In addition to SOA that was generated at variable C_{OA} , seven experiments involved the dilution
4 of SOA that was initially formed at high C_{OA} ($\geq 380 \mu\text{g m}^{-3}$) and diluted to low C_{OA} . The dilution
5 occurred downstream of the flowtube, charcoal denuder and ozone denuder. To achieve the desired
6 dilution the aerosol-laden airstream was divided into two fractions; one was directed through a
7 HEPA capsule filter with Versapor® membrane (Pall Corp.) to remove particles from the air
8 stream and the other passed directly through 1/8-in copper tubing. The two air streams were
9 recombined after the filter and passed directly to the TD. The fraction of the airstream directed
10 through the HEPA filter, i.e. the level of dilution, was controlled by a needle valve attached to the
11 outlet of the filter.

12 **2.2 Thermodenuder**

13 The TD used here is based on the design of Huffman et al. (2008) with the following key
14 modifications: 1) the heated laminar flow reactor is 0.71 m long (as compared to 0.41 m) and has
15 a center line fully-heated residence time (τ_{res}) of 26 seconds at a flow rate of 0.40 lpm; 2) the
16 distance between the actively heated volume and the charcoal denuder has been shortened and is
17 now 4.8 cm (as compared to ~14 cm); 3) there is only one heating region. The shorter distance
18 between the end of the actively heated volume and the charcoal denuder helps to limit re-
19 condensation as the air cools prior to reaching the denuder section. The bypass (i.e. unheated) line
20 had the same volume as the TD, and thus the same total residence time. Further information on the
21 design and characterization of the TD is provided in the *Supplemental Information*. The room
22 temperature flowrate through the TD was a constant 0.40 lpm independent of the total flowrate in
23 the SOA formation flowtube. Measurements of the particle size distribution were made after the
24 particles passed through either the bypass line (room temperature) or the TD. The TD temperature
25 ranged from room temperature (298 K) to 220°C (493 K). No differences in the mass thermograms
26 were found between experiments based on the order of temperature changes, e.g. whether
27 temperature was increased or decreased.

28

29

1 2.3 Measurements

2 A scanning mobility particle sizer (SMPS; TSI, Inc.), composed of a charge neutralizer, a
3 differential mobility analyzer (DMA; Model 3085) and a condensation particle counter (CPC;
4 Model 3772), was used to measure particle size distributions. The extent of aerosol evaporation
5 was characterized by comparing the particle size distribution for particles that passed through the
6 bypass line to that for the particles after passing through the TD. The size distributions were
7 characterized by their volume-weighted median diameter, $d_{p,V}$. The particle volume fraction
8 remaining (VFR) after passing through the TD is then:

$$9 \quad VFR = \frac{\frac{\pi}{6}d_{p,V,TD}^3}{\frac{\pi}{6}d_{p,V,bypass}^3}, \quad (2)$$

11 where $d_{p,V,TD}$ and $d_{p,V,bypass}$ refer to the particles that passed through the TD or the bypass,
12 respectively. Under an assumption of constant particle density, the VFR is equivalent to the
13 particle mass fraction remaining (MFR), and plots of VFR versus temperature are commonly
14 referred to as mass thermograms. The bypass distribution was measured at least every two
15 temperature changes (~every 20 minutes) to account for any changes in the reference particle
16 distribution; in general, the reference distributions were very stable.

18 To facilitate quantitative comparison between experiments at different CO_A , each mass
19 thermogram was fit to the sigmoidal type equation from Emanuelsson et al. (2013):

$$20 \quad VFR(T) = VFR_{max} + \left(\frac{VFR_{min} - VFR_{max}}{1 + \left(\frac{T_{50}}{T}\right)^{S_{VFR}}} \right), \quad (3)$$

22 where VFR_{min} is the VFR at the low temperature limit, VFR_{max} is the VFR at the high temperature
23 limit (typically zero), S_{VFR} is the slope factor that characterizes the steepness of the VFR curve and
24 T_{50} is the temperature at which $VFR = 0.50$. If there is no evaporation in the TD at room
25 temperature due to the removal of gas-phase compounds (vapor stripping) in the denuder section
26 then the VFR at room temperature (298 K) should be, by definition, unity. Best-fit VFR_{min} values
27

1 greater than unity may, however, be obtained because Eqn. 3 is an empirical expression and thus
2 is not expected to provide a perfect match with the observations, although can nonetheless facilitate
3 comparison between different experiments. Here, to provide for more consistent fitting and since
4 no evaporation was observed at room temperature, the fit curves were forced to go through unity
5 at room temperature.

6 **2.4 Kinetic Model of Evaporation**

7 **2.4.1 Thermodenuder model**

8 The kinetic model of evaporation used here is a modified version of the model developed by
9 Cappa (2010) to simulate evaporation in a thermodenuder. The original model simulated
10 gas/particle mass transfer (evaporation and condensation) for a monomodal multi-component
11 aerosol as particles pass through and are heated and cooled in the TD along with loss of vapors to
12 the charcoal denuder. Absorptive partitioning is implicitly assumed. Compounds evaporate
13 according to their respective saturation vapor concentrations, and it is assumed that the gas/particle
14 system is at equilibrium before entering the TD. The temperature dependence of C^* is accounted
15 for using the Clausius-Clapeyron equation. Here, it is assumed that the enthalpy of vaporization,
16 ΔH_{vap} , is related to C^* according to the relationship of Epstein et al. (2010), where $\Delta H_{\text{vap}}(\text{kJ mol}^{-1})$
17 $= 131 - 11 \times \log C^*$. The temperature profile through the TD is empirically specified (see SI). The
18 key input to the model is the distribution of mass (gas + particle) with respect to C^* , referred to as
19 a volatility distribution; different distributions will yield different mass thermograms (Cappa and
20 Jimenez, 2010). It is commonplace to assume a distribution where the C^* values differ by an order
21 of magnitude at a specified reference temperature, e.g. $\log C^*(298 \text{ K}) = (-3, -2, -1, 0, 1, 2, 3)$, and
22 this approach is adopted here. The calculated mass transfer rates can be adjusted to account for
23 mass transfer limitations, as characterized by the evaporation coefficient, γ_e , which characterizes
24 deviations from the theoretical maximum evaporation rate; γ_e is an adjustable parameter as it is not
25 known *a priori*. The default value used is $\gamma_e = 1$. The model output for a given set of ΔH_{vap} and C^*
26 is dependent on γ_e . At smaller γ_e the slope of the mass thermogram is less steep, the T_{50} increases
27 and for SOA with semi-volatile components an increasing amount of mass remains after TD-
28 processing at room temperature (Cappa and Wilson, 2011). The model can be run with pre-
29 specified volatility distributions or can be used to determine empirical volatility distributions from
30 fitting to observations (Cappa and Jimenez, 2010).

1 The base TD model has been modified to include the influence of dimers and dimer
2 decomposition on the simulated evaporation, and shares some similarities with Trump and
3 Donahue (2014). The dimer model is implemented as follows. The initial equilibrium gas/particle
4 mass distribution is based on a semi-volatile monomer volatility distribution (i.e. that determined
5 from previous growth experiments). The balance between monomers and dimers at equilibrium is
6 then determined from the monomer/dimer equilibrium constant, K_{eqm} ($\text{cm}^3 \text{ molecules}^{-1}$), which is
7 equal to the ratio of the forward (k_f , $\text{cm}^3 \text{ molecules}^{-1} \text{ s}^{-1}$) and reverse (k_r , s^{-1}) rate coefficients
8 associated with formation from monomers and dimer decomposition, i.e. $K_{\text{eqm}} = k_f/k_r$. Note that
9 the volume units on K_{eqm} and k_f correspond to condensed-phase volume. If K_{eqm} is large then all
10 condensed-phase species would be in dimer form and, at equilibrium, all gas-phase material would
11 be drawn into the condensed phase, assuming that the monomers are miscible with the dimers.
12 Here, this situation is avoided through the following simplification to determine the initial particle
13 state at the TD inlet. First, the gas/particle (monomer only) equilibrium distribution is calculated
14 given the specified volatility distribution and C_{OA} . Then the monomer/dimer equilibrium in the
15 condensed phase only is calculated based on the current condensed-phase monomer
16 concentrations. The gas-phase concentrations are then set to zero to avoid large amounts of
17 condensing material at the next time step. Since a charcoal denuder is placed immediately after the
18 flowtube, this simplification is physically reasonable as we have previously found that vapor
19 stripping in charcoal denuders is efficient (Cappa and Wilson, 2011). The resulting monomer-
20 dimer concentrations in the condensed phase are used as the initial state. The above simplification
21 for the initial particle state most likely does not provide a true representation of the actual particle
22 composition, just as the assumption regarding only homodimers (discussed below) is a
23 simplification. However, as we ultimately find that the simulation results are much more sensitive
24 to the initial distribution of particulate mass with respect to monomers and dimers than to the
25 specific distribution of monomers with respect to their volatility, these simplifications will
26 influence the details but not the general conclusions arrived at here.

27 It is assumed that the dimers are non-volatile over the entire temperature range considered, and
28 thus do not directly evaporate. In addition, only homodimers, that is dimers formed from
29 monomers in the same volatility bin, are assumed to form. This is a simplification compared to
30 allowing for all possible cross-reactions and allows for more straight-forward keeping track of the
31 dimer source monomers. As the temperature increases within the TD the dimers decompose into

1 their semi-volatile parent monomers, which can then evaporate according to their saturation vapor
 2 concentration. It was assumed that there were no mass transport limitations within the
 3 particle-phase for all evaporating species, i.e. that the surface composition was always equivalent
 4 to the bulk composition. As the semi-volatile monomers evaporate the equilibrium state is
 5 perturbed and the dimers decompose in response, according to the temperature dependent K_{eqm} , to
 6 re-establish dimer/monomer equilibrium. Depending on the timescale of dimer formation and
 7 decomposition, the dimers and monomers may not be in equilibrium at every step of the model,
 8 yet they are constantly forming and decomposing to move towards equilibrium. Experimental
 9 observations by Hall and Johnston (2012b) have shown that dimers in SOA do decompose upon
 10 heating. The rate at which dimers decompose is governed by changes to k_r and k_f , as a function of
 11 temperature. Assuming they exhibit Arrhenius-type temperature dependence, the temperature
 12 sensitivity of K_{eqm} can be characterized by the difference in the activation energies of the reverse
 13 and forward reactions, $\Delta E_a = E_{a,r} - E_{a,f}$, and where the temperature dependence of k_r and k_f has the
 14 form:

$$16 \quad k_r(T) = k_r(298K) \cdot e^{\left(-\frac{E_{a,r}}{RT} + \frac{E_{a,r}}{R \cdot 298K}\right)} = A_r \cdot e^{-\frac{E_{a,r}}{RT}} \quad (4)$$

17
 18 where R is the universal gas constant (8.314 J mol⁻¹ K), T is the temperature (K) and where

$$20 \quad A_r = k_r(298K) \cdot e^{-\frac{E_{a,r}}{R \cdot 298}}. \quad (5)$$

21
 22 Note that the Arrhenius pre-factor, A_r , depends on $E_{a,r}$. Consequently,

$$24 \quad K_{eqm}(T) = \frac{k_r(298K)}{k_f(298K)} \cdot e^{-\frac{\Delta E_a}{R \cdot 298K}} \cdot e^{-\frac{\Delta E_a}{RT}} = \frac{A_r}{A_f} \cdot e^{-\frac{\Delta E_a}{RT}} \quad (6)$$

25
 26 and ΔE_a is as defined above. It should be noted that this formulation differs somewhat from that
 27 of Trump and Donahue (2014) in that they assumed that A and E_a were independent parameters

1 and further did not account for the T-dependence of k_f , which we account for here in the
2 relationship between k_r , k_f and ΔE_a . The key model inputs are then $K_{eqm}(298\text{ K})$, $k_r(298\text{ K})$ and
3 ΔE_a . Although K_{eqm} governs the equilibrium distribution, k_f and k_r will control the timescales
4 associated with dimer formation and the approach to equilibrium in the particles.

5 **2.4.2 Isothermal evaporation model**

6 The kinetic thermodenuder model of evaporation was adapted to allow for simulation of
7 particle evaporation at room temperature following from isothermal dilution for any initial input
8 of particle composition including semi-volatile monomers, very low volatility compounds and a
9 mixture of semi-volatile monomers and non-volatile dimers. The extent of dilution is user-
10 selectable as a dilution factor (DF), which simulates SOA and the associated vapors being passed
11 through a DMA and injected into a chamber. The organic vapors are assumed to be removed from
12 the system (i.e. lost to the chamber walls) with a rate characterized by a user-selectable first order
13 loss rate, k_{loss} (s^{-1}). Vapor loss serves to mimic the conditions in some isothermal evaporation
14 experiments where the diluted SOA particles are held in a chamber containing activated carbon
15 (Vaden et al., 2011). The timescales associated with isothermal evaporation are much longer than
16 for the TD experiments and simulations, and the isothermal evaporation model can be run for many
17 hours of model time. When the monomer/dimer equilibrium is used to establish the initial particle
18 composition, the relationships between K_{eqm} , k_r , k_f and ΔE_a are the same as in the TD evaporation
19 model.

20

21 **3 Results and Discussion**

22 **3.1 Observations**

23 Evaporation and shrinking of the α -pinene+O₃ SOA particles occurred upon heating in the TD.
24 Example size distributions as a function of temperature for an initial $C_{OA} = 9\ \mu\text{g m}^{-3}$ are shown in
25 Figure 1. The mass thermograms for each individual experiment are shown in Figure 2. The
26 experimental results have been grouped according to the bypass C_{OA} for each experiment, with
27 groupings of: (i) high, $C_{OA} > 300\ \mu\text{g m}^{-3}$; (ii) medium, $90 \leq C_{OA} < 300\ \mu\text{g m}^{-3}$; and low, $C_{OA} \leq 30\ \mu\text{g}$
28 m^{-3} . The demarcations were chosen based on the results from Shilling et al. (2009), who observed
29 that particle composition varied with C_{OA} . Results from experiments where SOA was formed at a

1 high C_{OA} ($>300 \mu\text{g m}^{-3}$) and then rapidly isothermally diluted to a lower concentration ($<30 \mu\text{g}$
2 m^{-3}) are also reported in Figure 2. Each experiment was individually fit according to Eq. 3, and the
3 best-fit parameters are given in Table S1. The average T_{50} and S_{VFR} for each C_{OA} grouping are
4 given in Table 2.

5 Within each grouping the mass thermograms are all very similar, especially for the low and
6 medium cases. No evaporation is observed at room temperature from vapor stripping in the
7 denuder section for any case. The maximum variability is observed within the high C_{OA} grouping,
8 although even here the variability is not particularly large, with the average and sample standard
9 deviation $S_{VFR} = 16.4 \pm 1.5$ and in $T_{50} = 359 \pm 7\text{K}$. The S_{VFR} 's for all groupings are statistically
10 indistinguishable, as are the T_{50} values for the low and medium groupings. However, the T_{50} for
11 the high C_{OA} grouping is significantly larger at the $p < 0.05$ level ($p = 0.006$ and $p = 0.025$ as
12 compared to the low and medium C_{OA} groupings, respectively, for a two-tailed test). Visual
13 inspection of Figure 2a indicates that one experiment, with $C_{OA} = 600 \mu\text{g m}^{-3}$, has a notably larger
14 T_{50} . If this experiment is excluded the $T_{50} = 357 \pm 5 \text{K}$, which is still statistically larger than the
15 low C_{OA} T_{50} at the $p < 0.05$ level ($p = 0.008$ for the two-tailed test) but is only now statistically
16 larger than the medium C_{OA} T_{50} at the $p < 0.10$ level ($p = 0.079$ for the two-tailed test). This
17 difference could be due to small amounts of re-condensation or to saturation of the gas-phase, both
18 of which become a greater concern at high C_{OA} (Cappa, 2010;Saleh et al., 2011;Cappa and
19 Jimenez, 2010;Fuentes and McFiggans, 2012;Riipinen et al., 2010), although there is no specific
20 dependence of T_{50} on C_{OA} within the high C_{OA} group. Regardless, it is apparent that the effective
21 volatility of the SOA at high C_{OA} is not higher than at low C_{OA} and that, despite the slight
22 differences, the response to heating of SOA particles formed from products of the ozonolysis of
23 α -pinene is, to a very large extent, independent of the C_{OA} at the point of formation. This then
24 suggests that, from a volatility perspective, the distribution of compounds in the particle is
25 independent of C_{OA} , which stands in contrast to expectations based on the growth-derived volatility
26 distribution.

27 The mass thermogram of SOA originally formed at high C_{OA} and isothermally diluted to low
28 C_{OA} was also measured (Figure 2d). Since the evaporation of SOA induced by isothermal dilution
29 occurs very slowly, on the order of many minutes to hours (Grieshop et al., 2007;Saleh et al.,
30 2013), the composition of the diluted SOA is not expected to change substantially from the initial

1 state of formation at high C_{OA} before the particles enter the TD. The T_{50} of the SOA formed at high
2 C_{OA} is larger than for the diluted SOA, and significantly different at the $p < 0.05$ level ($p = 0.003$
3 for a two-tailed test), while the average S_{VFR} of the diluted and the high C_{OA} grouping mass
4 thermograms are statistically indistinguishable at the $p < 0.05$ level ($p = 0.443$ for the two-tailed
5 test). This strongly suggests that the difference in T_{50} of the high C_{OA} grouping results from
6 re-condensation or saturation of the gas-phase, although the possibility that there is some real
7 difference in the effective volatility of particles after rapid isothermal dilution cannot be excluded.
8 The average diluted SOA mass thermogram is also almost identical to the average low C_{OA} mass
9 thermogram indicating that the volatility distributions of the compounds in the diluted and low
10 C_{OA} cases are the same. Overall, it is evident that the rapid dilution of SOA does not induce changes
11 to molecular composition that significantly influence particle volatility.

12 **3.2 Evaporation Modeling**

13 **3.2.1 Semi-volatile SOA model**

14 The observed similarity between the mass thermograms for the SOA formed at orders of
15 magnitude different C_{OA} is surprising given that some observations suggest that particle
16 composition depends on C_{OA} (e.g. Shilling et al. (2009)). Since the application of absorptive
17 partitioning theory to the interpretation of SOA growth experiments suggests that the particles are
18 (i) composed of compounds with a large distribution of individual volatilities, typically with C^*
19 values $> 10^{-1} \mu\text{g m}^{-3}$ and (ii) that the fraction of higher volatility compounds should increase with
20 increasing C_{OA} , the mass thermograms are expected to depend on C_{OA} . Using a volatility
21 distribution for α -pinene + O_3 SOA derived from SOA formation experiments (Pathak et al.,
22 2007), simulated mass thermograms have been calculated as a function of C_{OA} (for $\gamma_e = 1$ or 0.001)
23 using the TD model, first assuming that the particles are composed only of monomers (Figure 3).
24 Results from this model will be referred to as semi-volatile monomer results. Specifically, we use
25 the 7-bin volatility distribution with $\log C^* = [-2, -1, 0, 1, 2, 3, 4]$ and mass yields of $\alpha = [0.001, 0.012,$
26 $0.037, 0.088, 0.099, 0.250, 0.800]$. The theoretical mass thermograms, for $\gamma_e = 1$, indicate that a
27 significant dependence of the mass thermograms on C_{OA} should have been observed (Figure 3a).
28 Further, they indicate that substantial evaporation of the SOA particles at high C_{OA} should have
29 been observed at room temperature due to vapor stripping in the charcoal denuder section of the
30 TD, which occurs to some extent for any species with $C^* \geq \sim 1 \mu\text{g m}^{-3}$ when $\gamma_e = 1$. Neither of these

1 phenomena were observed, demonstrating that there is a clear disconnect between typical volatility
2 distributions derived from SOA growth experiments and SOA evaporation experiments, as has
3 previously been noted (e.g. (Cappa and Jimenez, 2010)).

4 Some measurements of time-dependent evaporation profiles of SOA have been interpreted as
5 suggesting that γ_e is significantly less than unity for α -pinene + O₃ SOA due to mass transfer
6 limitations in the condensed phase (Grieshop et al., 2007; Saleh et al., 2013; Karnezi et al., 2014).
7 Further, some TD-based SOA studies have used γ_e as a tunable parameter in data fitting for
8 individual experiments and suggest that $\gamma_e < 1$ (Lee et al., 2011; Lee et al., 2010). Therefore, model
9 predictions for C_{OA} dependent mass thermograms are also reported for $\gamma_e = 0.001$ (Figure 3b). As
10 expected, the apparent volatility (i.e. extent of evaporation at a given temperature) is decreased
11 compared to the $\gamma_e = 1$ case, and the simulated thermograms exhibit a greater similarity to the
12 observations. Also, the extent of evaporation at room temperature is substantially lowered and
13 more consistent with the observations, as now only species with $C^* \geq \sim 1000 \mu\text{g m}^{-3}$ will evaporate
14 to any substantial extent in the TD due to vapor stripping alone. However, the simulations also
15 indicate a very strong C_{OA} dependence — higher volatility with higher C_{OA} — is expected when
16 $\gamma_e = 0.001$, which is inconsistent with the observations here. This demonstrates that conclusions
17 regarding the magnitude of parameters such as γ_e when derived from single experiments may not
18 provide a robust description of the process in question (here, evaporation) because they are not
19 unique solutions (i.e. are dependent on the other model inputs, namely the assumed ΔH_{vap} and
20 volatility distribution). Regardless of assumptions about mass transfer limitations, the model
21 predictions for the mass thermograms of particles comprised entirely of monomers (i.e. based on
22 the Pathak et al. (2007) volatility distribution) unambiguously show a dependence on C_{OA}. Thus,
23 there is a clear disconnect between volatility distributions derived from SOA growth experiments
24 and observations from SOA evaporation experiments that cannot be entirely explained by kinetic
25 limitations to evaporation.

26 **3.2.1 Dimer-Decomposition Model**

27 The above discrepancy strongly suggests that the molecular composition of the condensed
28 phase is only indirectly related to the volatilities of the condensing species as determined from
29 growth experiments. Here, the possibility that this discrepancy can be explained through the

1 formation and subsequent decomposition of dimers (and higher-order oligomers) through
2 condensed phase reactions is examined. Cappa and Wilson (2011) demonstrated that, although
3 simple applications of equilibrium absorption partitioning theory can explain SOA growth in
4 laboratory chamber experiments, such models are not unique explanations. In particular, they
5 showed it was possible to reconcile SOA growth experiments with the occurrence of condensed-
6 phase reactions—even to the extent that the entire particle is rapidly converted from monomers
7 (that retain the volatility of the condensing species) to non-volatile species. There is now a variety
8 of experimental evidence that many types of SOA particles are composed of a large fraction of
9 oligomers (Kourtchev et al., 2014;Putman et al., 2012;Kundu et al., 2012;Gao et al., 2004a;Muller
10 et al., 2009;Kalberer et al., 2004), which will generally have volatilities lower than the monomeric
11 precursors. For the system considered in this study, α -pinene + O₃ SOA, the oligomeric content is
12 suggested to be greater than 50% (Tolocka et al., 2004;Gao et al., 2004a;Gao et al., 2004b;Hall
13 and Johnston, 2012a) and both laboratory (Kristensen et al., 2014) and ambient (Kristensen et al.,
14 2013;Yasmeen et al., 2010) measurements have identified several α -pinene+O₃ SOA dimers.

15 Simulated mass thermograms have been calculated as a function of C_{OA} using the modified
16 TD model, in which some fraction of the condensed-phase material is assumed to exist as dimers.
17 The same 7 volatility bins were used with the same mass yields as the semi-volatile monomer case
18 to calculate the initial concentration of monomers in the particle. As described above, the
19 equilibrium coefficient, K_{eqm} , was used to determine the initial monomer/dimer equilibrium while
20 the decomposition rate coefficient, k_r , and activation energy, ΔE_a , describe the rate and sensitivity
21 to temperature changes of dimer thermal decomposition. None of the parameters are known *a*
22 *priori*. Since there is a relationship between all three parameters ($K_{eqm} = k_i/k_r$ and $k_r(T)$ are
23 dependent on ΔE_a) we have taken the approach of specifying different values of K_{eqm} and then
24 fitting the model to the observations by adjusting k_r and ΔE_a . The level of model/measurement
25 agreement for the different K_{eqm} was then assessed.

26 The model aerosol used had $d_p = 90$ nm and $C_{OA} = 100$ $\mu\text{g m}^{-3}$ as starting conditions, and was
27 fit to the average mass thermogram of the medium/low C_{OA} grouping (Figure 4a). Generally good
28 fits were obtained for all K_{eqm} over the range 10^{-18} to 10^{-14} $\text{cm}^3 \text{ molecule}^{-1}$, with the overall best
29 agreement obtained for $K_{eqm} = 10^{-17}$ $\text{cm}^3 \text{ molecule}^{-1}$, although the differences are quite small (see
30 the *SI* for the best-fit model parameters for each K_{eqm}). At smaller K_{eqm} , extensive room

1 temperature evaporation occurred as a result of the increasing initial fraction of semi-volatile
2 monomers, a result that is inconsistent with the observations. However, even for the simulations
3 at larger K_{eqm} , some evaporation at room temperature was always predicted. The simulated room
4 temperature evaporation at larger K_{eqm} may result from the model assumption of liquid-like
5 particles in that if mixing within the particles were slow such that there were a build up at the
6 particle surface of non-volatile dimers then evaporation of monomers that are buried below the
7 surface would be slowed (Roldin et al., 2014). The associated best fit $k_r(298 \text{ K})$ and ΔE_a varied
8 with K_{eqm} , from $1.6 \times 10^{-3} \text{ s}^{-1}$ to $2.8 \times 10^{-2} \text{ s}^{-1}$ and from 15 kJ/mol to 42 kJ/mol, respectively; smaller
9 K_{eqm} values corresponded to larger k_r and smaller ΔE_a .

10 These K_{eqm} values correspond to a case where the particles are almost entirely composed of
11 dimers, as the dimer fraction is >97% for all $K_{\text{eqm}} > 10^{-18} \text{ cm}^3 \text{ molecule}^{-1}$. The range of best-fit k_r
12 indicate a dimer lifetime of only 1-10 minutes with respect to decomposition at room temperature.
13 The range of k_f values associated with the best fit K_{eqm} and k_r is 1.6×10^{-21} to $2.8 \times 10^{-16} \text{ cm}^3$
14 $\text{molecules}^{-1} \text{ s}^{-1}$. Given a typical molecular density of $\sim 10^{21} \text{ molecules cm}^{-3}$, the approximate dimer
15 formation timescale is only a fraction of a second, consistent with the short reaction time in these
16 experiments. Consequently, the dimer decomposition timescale is not the same as the observable
17 timescale associated with particle mass loss at room temperature upon e.g. isothermal dilution
18 (Grieshop et al. (2007)). However, there are several potential factors that slow down evaporation
19 at room temperature despite the short dimer lifetime with respect to decomposition, as discussed
20 below when isothermal dilution and evaporation is considered. The K_{eqm} , k_r , and ΔE_a determined
21 above from fitting the medium/low C_{OA} data (i.e. $C_{\text{OA}} = 100 \mu\text{g m}^{-3}$) have been used to predict
22 additional mass thermograms for $C_{\text{OA}} = 1, 10, 70$ and $600 \mu\text{g m}^{-3}$ (Figure 5a). The predicted mass
23 thermograms are mostly independent of C_{OA} , in contrast with the semi-volatile monomer model.
24 Thus, when the particle is nearly entirely initially dimers this “dimer-decomposition” model result
25 is generally consistent with the experimental observations, where limited differences were
26 observed between the mass thermograms measured at different C_{OA} , although it should be noted
27 the slight increase in T_{50} observed at the highest mass loadings is not reproduced. Also, only the
28 $C_{\text{OA}} = 1 \mu\text{g m}^{-3}$ simulation predicts negligible evaporation at room temperature, as was observed
29 for all C_{OA} . The dimer-decomposition model also predicts that the observable particle composition
30 should remain relatively constant as evaporation is induced (Figure 6a), consistent with

1 observations. This prediction is consistent with previous measurements in which it was observed
2 that the particle composition, as measured using a vacuum ultraviolet aerosol mass spectrometer
3 (VUV-AMS) remained quite constant during the heating induced evaporation of α -pinene+ O₃
4 SOA (Cappa and Wilson, 2011). There are several experiments where changes to composition
5 were observed. Hall and Johnston (2012b) used an electrospray ionization Fourier transform ion
6 cyclotron resonance (ESI-FTICR) mass spectrometer to measure the fraction of oligomers in the
7 particle before and after heating (393 K) and found that the fraction of oligomers and the O:C ratio
8 increase after heating. Furthermore, when re-condensation does occur, the compounds that
9 recondensed appear to be monomer decomposition products. Kostenidou et al. (2009) used a
10 quadrupole AMS to quantify the mass fraction of m/z 44 fragments as a function of MFR and
11 found that the fraction of m/z 44 increased as MFR decreased, indicating more oxygenated
12 particles with heating-induced evaporation. Since the dimer model presented here tracks the
13 relative concentration of dimers and monomers due to decomposition, the most comparable study
14 is Cappa and Wilson (2011) because the measurement technique is one that primarily detects the
15 monomer components due, most likely, to thermal degradation during analysis.

16 Trump and Donahue (2014) and Roldin et al. (2014) have previously suggested that accounting
17 for the behavior of dimers within SOA can help to explain observations of SOA evaporation; our
18 observations and analysis support and expand upon this conclusion. The range of k_f independently
19 determined here are somewhat larger than the room-temperature k_r suggested by Trump and
20 Donahue (2014) ($=1.1 \times 10^{-4} \text{ s}^{-1}$) and Roldin et al. (2014) ($=2.8 \times 10^{-5} \text{ s}^{-1}$), which were based on
21 needing an evaporation timescale of ~ 1 hr for isothermal evaporation (Grieshop et al., 2007; Vaden
22 et al., 2011). Ultimately, reconciliation of the different timescales indicated for dimer
23 decomposition between the different studies likely will require more detailed consideration of the
24 exact nature of various dimer types with respect to their decomposition and formation timescales,
25 which may not all be identical as assumed here, and of the influence of particle phase on
26 evaporation. It should be noted that the ΔE_a determined here are substantially smaller than that
27 suggested by Trump and Donahue (2014), who give $E_{a,r} \sim 80 \text{ kJ mol}^{-1}$ (and where, it seems, that
28 their $E_{a,r}$ is essentially equal to the ΔE_a here as they assume that k_f is T-independent). However,
29 this difference can be understood by recognizing that they assumed a constant value for A ($= 3 \times$
30 10^{10} s^{-1}) and $k_f(300 \text{ K})$ and determined $E_{a,r}$ using the relationship $k_f(T) = A \exp(-E_{a,r}/RT)$. Thus,

1 underestimations of k_r may lead them to actually overestimate the true temperature sensitivity of
2 the system.

3 The best-fit K_{eqm} and k_r were determined from fitting to T-dependent evaporation experiments
4 that occur over relatively short timescales (~ 1 min) in the thermodenuder. To facilitate more direct
5 connections with previous experiments that have investigated room temperature evaporation upon
6 dilution, the best-fit dimer-decomposition model for $K_{\text{eqm}} = 10^{-17} \text{ cm}^3 \text{ molecules}^{-1}$ has been used
7 to simulate the long-time, isothermal, room-temperature evaporation of SOA for the case where
8 the SOA is initially diluted and the evaporating vapors are constantly being stripped from the gas-
9 phase (Figure 4b). This corresponds approximately to the conditions in a series of experiments
10 investigating SOA evaporation (Vaden et al., 2011; Wilson et al., 2015). A vapor loss rate constant
11 of $k_{\text{loss}} = 10^{-3} \text{ s}^{-1}$ has been used, which is a reasonable estimate given the size of the chambers used
12 in the previous experiments (Matsunaga and Ziemann, 2010; Zhang et al., 2014). The initial (pre-
13 dilution) $C_{\text{OA}} = 100 \mu\text{g m}^{-3}$, which was diluted by a factor of $DF = 30$ to induce evaporation.

14 The literature experiments have generally shown evidence for evaporation of SOA on fast,
15 medium and slower timescales, where “fast” corresponds to timescales of around a minute,
16 “medium” corresponds to timescales of around 1 hour and “slow” to timescales of many hours.
17 The dimer model simulations for all the K_{eqm} fits exhibit similar behavior, with “fast,” “medium”
18 and “slow” periods of mass loss and timescales similar to previous observations. There is a non-
19 monotonic dependence on K_{eqm} , with the least mass loss predicted for $K_{\text{eqm}} = 10^{-16} \text{ cm}^3 \text{ molecules}^{-1}$
20 and greater total mass loss predicted for K_{eqm} both larger and smaller. The behavior results from a
21 balance between the k_r , k_f and evaporation time scales for each K_{eqm} fit. After 15 h the simulated
22 MFR of SOA is 5-27% of the initial (post-dilution) C_{OA} . The general model behavior, which
23 indicates that evaporation occurs on multiple timescales, can be understood by recognizing that
24 decomposition of dimers composed of higher C^* monomers leads to rapid evaporation, such that
25 the observable evaporation rate is controlled by the dimer decomposition. In contrast,
26 decomposition of dimers composed of lower C^* monomers results in species that do evaporate,
27 but only slowly at room temperature. Given a distribution of monomers with respect to their C^* ,
28 the result is a time-dependent evaporation profile multiple apparent timescales for evaporation.
29 Further, as evaporation proceeds, the finite rate of vapor loss means that over time the gas-phase
30 concentration may build up, which will also limit the rate of mass loss.

1 The simulated MFR values at the end of 15 h of SOA evaporation are somewhat lower than
2 was observed in the literature experiments for dry, fresh SOA from α -pinene + O₃, where MFR ~
3 0.35-0.4 at 15 h (Vaden et al., 2011; Wilson et al., 2015). However, the extent of evaporation is
4 dependent on the model assumptions, specifically the k_{loss} and DF . Smaller k_{loss} or DF leads to
5 larger MFR at a given time due to more extensive inhibition of evaporation resulting from faster
6 saturation of the gas-phase (Figure 7a). Conversely, larger k_{loss} or DF lead to more extensive
7 evaporation. As neither the k_{loss} nor DF are explicitly known for the literature experiments, a more
8 quantitative comparison is not possible. However, it is nonetheless noteworthy that the model
9 suggests that both k_{loss} and DF can play a controlling role in observations of isothermal
10 evaporation. These previous isothermal evaporation measurements also indicate that SOA
11 evaporation is mostly size independent, in contrast to evaporation of single-component particles
12 (Vaden et al., 2011; Wilson et al., 2015). Simulations using the dimer-decomposition model with
13 different starting particle sizes show some dependence on particle size ($d_p = 90, 180$ and 360 nm),
14 with larger particles having smaller MFRs at a given time (Figure 7a). However, the overall
15 differences are relatively small and reasonably consistent with the observations given that the
16 observations have typically considered a narrower size range than examined here.

17 **3.2.1 Low-volatility SOA Model**

18 One alternative possibility to explain the observations of evaporation of SOA in the TD is that
19 the observed heating-induced evaporation results from direct evaporation of low-volatility species.
20 These low-volatility species could be either highly oxygenated monomers (Ehn et al., 2014) or
21 thermally-stable dimers or higher-order oligomers, although the thermal stability of dimers seems
22 unlikely (Hall and Johnston, 2012a). To test this idea, the TD model has been fit to the observations
23 assuming that the particles are only composed of semi- and low-volatility species, but where the
24 volatility distribution is skewed to much lower C^* than suggested from SOA growth experiments
25 (i.e. from the Pathak et al. (2007) volatility distribution). Given that there is negligible evaporation
26 observed at room temperature in the TD for all C_{OA} , including $C_{\text{OA}} = 1 \mu\text{g m}^{-3}$, the highest volatility
27 bin was set at $C^* = 1 \mu\text{g m}^{-3}$. The lowest value was set based on the requirement that there remains
28 some particle mass at ~ 343 K. If ΔH_{vap} is too large then even very low-volatility compounds will
29 not persist to such high temperatures (Cappa and Jimenez, 2010; Cappa, 2010). As such, an upper-
30 limit ΔH_{vap} constraint of 185 kJ mol^{-1} was placed on the $C^*/\Delta H_{\text{vap}}$ parameterization, and a lower

1 bound C^* of $10^{-9} \mu\text{g m}^{-3}$ was used. Following Cappa and Jimenez (2010), a relationship between
2 the total organic mass and C^* was assumed, where $C_{i,\text{tot}} = a_1 + a_2 \exp[a_3(\log(C^*) + a_4)]$. Values of
3 the a_x parameters have been determined through data fitting; it is difficult to constrain the absolute
4 C_{OA} while determining the a_x parameters through fitting, and thus C_{OA} was allowed to vary. The
5 model was fit to the average thermogram for the medium/low C_{OA} grouping, and a good fit was
6 found when the $a_x = [1.53, 8.5, 0.3, 0.59]$, with a corresponding C_{OA} of $71 \mu\text{g m}^{-3}$ (Figure 4a). This
7 demonstrates that an alternative model can potentially be used to explain the TD results, namely
8 one in which the condensed-phase species are very low volatility but evaporate directly in response
9 to heating.

10 If the same a_x distribution is used, but with $C_{i,\text{tot}}$ scaled up or down to give a different initial
11 C_{OA} (and slightly different distribution of compounds), the simulated volatility decreases slightly
12 as C_{OA} increases (Figure 5b). This is mostly due to gas-phase saturation at higher concentrations,
13 and subsequently greater re-condensation as the SOA cools in the denuder. Nonetheless, this is
14 opposite the C_{OA} dependence predicted by the semi-volatile monomer model and is in the same
15 direction of the observations, where the high C_{OA} grouping exhibited lower apparent volatility.
16 There is, however, some difference in the simulated mass thermograms for low and medium C_{OA} ,
17 which was not observed, although the gap between the low ($1\text{-}10 \mu\text{g m}^{-3}$) and medium ($100 \mu\text{g}$
18 m^{-3}) C_{OA} simulations is smaller than the gap between the medium and high ($600 \mu\text{g m}^{-3}$) C_{OA}
19 simulations. If re-condensation of the evaporated species were, for some reason, not particularly
20 efficient (due perhaps to changes in the molecular composition upon heating) then the differences
21 between the different C_{OA} simulations would be lessened.

22 As with the dimer-decomposition model, simulation of isothermal evaporation by the low-
23 volatility monomer model provides evidence for multiple evaporation timescales, with “fast,”
24 “medium” and “slow” components (Figure 4b). For the same $k_{\text{loss}} (= 10^{-3} \text{ s}^{-1})$ and $DF (= 30)$, the
25 extent of evaporation from the low-volatility aerosol simulation at 15 h is less than for the various
26 dimer-decomposition simulations. The low-volatility aerosol model exhibits a similar sensitivity
27 to the assumed k_{loss} and DF , and a slightly smaller sensitivity to changes in particle size (Figure
28 7b). It is apparent that the low-volatility aerosol model is compatible with the observations from
29 both our TD and the literature isothermal evaporation experiments (Vaden et al., 2011; Wilson et
30 al., 2015).

1 Although both the low-volatility aerosol and dimer-decomposition models perform equally
2 well in explaining the observed mass thermograms and literature observations of isothermal
3 evaporation, there is a distinct difference between two model results in terms of how the particle
4 composition is predicted to vary with temperature. Unlike the dimer-decomposition model, the
5 predicted relative particle composition undergoes substantial changes as the particles evaporate
6 upon heating for the low-volatility aerosol model (Figure 6b). This model result would suggest
7 that potentially large changes in composition should be observed upon heating or, more
8 generically, evaporation. This prediction is inconsistent with the various observations that suggest
9 negligible to very moderate changes in the observed particle composition (Cappa and Wilson,
10 2011;Kostenidou et al., 2009).

11 **3.2.1 Comparison between model results**

12 Overall, the dimer-decomposition model of evaporation provides the most comprehensive
13 explanation in that it can explain not only the current results where the observed mass thermograms
14 are nearly independent of C_{OA} , but also the minor changes in composition that occur upon heating-
15 induced evaporation of α -pinene+O₃ SOA observed by some (Cappa and Wilson, 2011), the
16 moderately long timescales required for achieving equilibrium upon isothermal dilution (Grieshop
17 et al., 2007) and the bimodality of SOA evaporation upon rapid dilution and subsequent continuous
18 vapor stripping (Vaden et al., 2011). The low-volatility monomer evaporation model can reproduce
19 many of these observations, but suggests large compositional changes upon heating. The semi-
20 volatile monomer model fails to reproduce nearly all of the observations. Additionally, the dimer-
21 decomposition model is potentially consistent with suggestions that SOA particles formed under
22 dry conditions have very high viscosity (Kannosto et al., 2013;Virtanen et al., 2010;Abramson et
23 al., 2013). The viscosity of SOA should decrease rapidly as temperature increases and, to the extent
24 that SOA might actually be a glass, could go through a glass-liquid transition (Koop et al., 2011).
25 If the particles were primarily semi-volatile monomers for which evaporation were limited by
26 diffusion in the particle phase, then decreases in viscosity should lead to substantial increases in
27 the observed evaporation rate (Zaveri et al., 2014;Roldin et al., 2014). The continuous change in
28 VFR with temperature out to relatively high temperatures suggests that the condensed-phase
29 species must have low-volatility such that as the viscosity decreases there is no substantial impact
30 on the observed particle evaporation. This model/observation comparison suggests that for SOA—

1 at least that produced from the α -pinene+O₃ reaction—the mass thermogram does not give direct
2 information on the distribution of volatilities of the original condensing compounds (i.e. the
3 monomers), but on the properties of the oligomers, specifically their thermal stability. One
4 limitation of the current kinetic model is the assumption that k_r and ΔE_a are the same for all dimers,
5 whereas it is likely that the rate and temperature-sensitivity of oligomer decomposition is
6 compound specific (Hall and Johnston, 2012b). However, expansion of the model to include such
7 information would only add more tunable parameters, but would not materially influence the
8 conclusions here.

9 Despite the general success of the dimer-decomposition model in reproducing a variety of
10 observations, it does predict some particle evaporation at room temperature in the TD, which was
11 not observed. Further, it seems unlikely that all particle mass is converted to dimers on such rapid
12 timescales as implied by the dimer-decomposition model; although accurate quantification of the
13 relative fractions of dimers (and larger oligomers) versus monomers in SOA particles has proven
14 challenging, it seems likely that the oligomer fraction is not 100% (Hall and Johnston,
15 2012b;Kalberer et al., 2004;Kristensen et al., 2014), some experiments have observed apparent
16 variations in VFR, determined from either heating or vapor stripping, as the particles are “aged”
17 by sitting in the dark (Abramson et al., 2013) or by exposure to oxidants (Kalberer et al., 2004;Salo
18 et al., 2011;Emanuelsson et al., 2013), suggesting that compositional changes (including dimer or
19 oligomer formation) may occur on multiple timescales, ranging from seconds to minutes to hours.
20 It therefore seems likely that a more complete representation of α -pinene+O₃ SOA volatility is
21 some hybrid of the dimer-decomposition and low-volatility species frameworks, where some
22 substantial fraction of the condensed phase mass exists as very low-volatility, effectively non-
23 volatile, dimers or oligomers — or even thermally-unstable, low-volatility monomers — that
24 decompose to produce species with a distribution of volatilities that subsequently evaporate, while
25 some fraction exists as low-volatility ($C^* < 1 \mu\text{g m}^{-3}$) species that can directly evaporate but for
26 which the actual volatilities tend to be lower than those predicted from traditional analyses of
27 growth experiments. Regardless of the details, the effective volatility of α -pinene+O₃ is much less
28 than predicted by growth experiments.

29 **4 Conclusions**

1 Experimental observations of T-dependent SOA evaporation have been presented that
2 demonstrate that the apparent volatility of α -pinene + O₃ SOA, as characterized by heating in a
3 thermodenuder, is mostly independent of the SOA concentration over many orders of magnitude
4 variation. Comparison of these observations with various kinetic models of evaporation in the TD
5 suggest the observations are most consistent with SOA from the ozonolysis of α -pinene being
6 composed of a large fraction of effectively non-volatile, but thermally-unstable species; these
7 species are likely dimers or higher order oligomers, but could also be exceptionally low-volatility
8 monomers. Any monomers that do exist must be of sufficiently low volatility ($< \sim 1 \mu\text{g m}^{-3}$) that
9 they do not readily evaporate at room temperature. A dimer-decomposition model provided a good
10 fit to the experimental observations when the monomer/dimer equilibrium constant ranged from
11 $K_{\text{eqm}} \sim 10^{-18}$ to $10^{-14} \text{ cm}^3 \text{ molecule}^{-1}$, with corresponding rate coefficients for the reverse
12 (decomposition) reaction ranging from $k_r(298\text{K}) = 1.6 \times 10^{-3}$ to $2.8 \times 10^{-2} \text{ s}^{-1}$, and a difference in
13 activation energies between the forward and reverse rate coefficients ranging from $\Delta E_a = 15$ to 42
14 kJ mol^{-1} . The best-fit dimer-decomposition model can also explain observations of slow rates of
15 evaporation after isothermal dilution (Vaden et al., 2011; Wilson et al., 2015) and nearly constant
16 composition as a function of rapid heating (Cappa and Wilson, 2011). These parameters would,
17 by themselves, suggest that the SOA particles are nearly entirely composed of dimers, which seems
18 unlikely. A model where the particle was assumed to be composed of low-volatility compounds
19 — either highly oxygenated monomers or oligomers — could explain the bulk evaporation
20 observations nearly as well, although suggested that large changes to particle composition upon
21 heating should be observed. Thus, it seems that a hybrid model where the particles are composed
22 of a substantial fraction of dimers (or oligomers) and some smaller fraction of low-volatility
23 compounds may ultimately provide a more complete description.

24 Many laboratory (Cappa and Wilson, 2011; Emanuelsson et al., 2013; Loza et al.,
25 2013; Grieshop et al., 2007; Saleh et al., 2013) and field studies (Cappa and Jimenez, 2010) have
26 aimed to characterize the volatility of SOA. In general, the observations have concluded that the
27 effective volatility of SOA is much lower than the volatility determined from interpretation of
28 formation studies within a gas/particle partitioning framework. The analysis presented here
29 suggests that this apparent discrepancy can be reconciled to a large extent through a combined
30 framework in which the volatility distributions derived from growth experiments (i.e. (Pathak et
31 al., 2007)) provides a reasonable description of the properties of the condensing monomers, but

1 where rapid formation of thermally-unstable dimers (and higher order oligomers) occurs, which
2 consequently suppresses the apparent volatility of the SOA. Since the residence time in our
3 flowtube was ~ 1 minute, these accretion reactions must occur on a similar timescale (or faster).
4 This dimer formation timescale is much faster than what is typically used within air quality models
5 (Carlton et al., 2010), which assume timescales on the order of a day, and suggests that air quality
6 models may therefore have SOA that is too volatile and thus overly sensitive to dilution. However,
7 care must be taken in the implementation of any model that allows for such rapid formation of
8 dimers, as the ultimate consequence would be to transfer all semi-volatile material to the
9 condensed phase. One possible reconciliation is that SOA particles may actually have a very high
10 viscosity (which is, perhaps, a consequence of oligomer formation), which can limit the transport
11 of gas-phase material into the particle bulk and the timescale and extent of transfer of gas-phase
12 material into the particles (Zaveri et al., 2014). Although the oligomeric content of ambient
13 biogenic SOA may be less than in laboratory biogenic SOA (Kourtchev et al., 2014) the presence
14 of oligomers has been observed in both and needs to be accounted for in models of SOA volatility.

15

16 **Author Contribution**

17 K.R. Kolesar and C.D. Cappa designed the experiments and D. Johnson carried them out. C.
18 Chen characterized the temperature profile in the thermodenuder. C.D. Cappa and K.R. Kolesar
19 modified the kinetic model of evaporation from Cappa (2010) and performed the simulations. K.R.
20 Kolesar and C.D. Cappa prepared the manuscript.

21

22 **Acknowledgements**

23 Special thanks to Anthony Kong for his assistance in running laboratory experiments. Funding
24 for this work was provided by the National Science Foundation (ATM-1151062). K.R.K. was
25 partially supported by a fellowship from the UC Davis Atmospheric Aerosols and Health program.

26

27

28 **References**

1 Abramson, E., Imre, D., Beranek, J., Wilson, J., and Zelenyuk, A.: Experimental determination of
2 chemical diffusion within secondary organic aerosol particles, *Physical Chemistry Chemical*
3 *Physics*, 15, 2983-2991, 10.1039/c2cp44013j, 2013.

4 Andreae, M. O., and Crutzen, P. J.: Atmospheric aerosols: Biogeochemical sources and role in
5 atmospheric chemistry, *Science*, 276, 1052-1058, 10.1126/science.276.5315.1052, 1997.

6 Cappa, C. D.: A model of aerosol evaporation kinetics in a thermodenuder, *Atmospheric*
7 *Measurement Techniques*, 3, 579-592, 10.5194/amt-3-579-2010, 2010.

8 Cappa, C. D., and Jimenez, J. L.: Quantitative estimates of the volatility of ambient organic
9 aerosol, *Atmospheric Chemistry and Physics*, 10, 5409-5424, 10.5194/acp-10-5409-2010, 2010.

10 Cappa, C. D., and Wilson, K. R.: Evolution of organic aerosol mass spectra upon heating:
11 implications for OA phase and partitioning behavior, *Atmospheric Chemistry and Physics*, 11,
12 1895-1911, 10.5194/acp-11-1895-2011, 2011.

13 Carlton, A. G., Bhawe, P. V., Napelenok, S. L., Edney, E. D., Sarwar, G., Pinder, R. W., Pouliot,
14 G. A., and Houyoux, M.: Model Representation of Secondary Organic Aerosol in CMAQv4.7,
15 *Environmental Science & Technology*, 44, 8553-8560, 10.1021/es100636q, 2010.

16 Chen, Y. Y., Ebenstein, A., Greenstone, M., and Li, H. B.: Evidence on the impact of sustained
17 exposure to air pollution on life expectancy from China's Huai River policy, *Proceedings of the*
18 *National Academy of Sciences of the United States of America*, 110, 12936-12941,
19 10.1073/pnas.1300018110, 2013.

20 Donahue, N. M., Robinson, A. L., Stanier, C. O., and Pandis, S. N.: Coupled partitioning, dilution,
21 and chemical aging of semivolatile organics, *Environmental Science & Technology*, 40, 02635-
22 02643, 10.1021/es052297c, 2006.

23 Ehn, M., Thornton, J. A., Kleist, E., Sipila, M., Junninen, H., Pullinen, I., Springer, M., Rubach,
24 F., Tillmann, R., Lee, B., Lopez-Hilfiker, F., Andres, S., Acir, I.-H., Rissanen, M., Jokinen, T.,
25 Schobesberger, S., Kangasluoma, J., Kontkanen, J., Nieminen, T., Kurten, T., Nielsen, L. B.,
26 Jorgensen, S., Kjaergaard, H. G., Canagaratna, M., Maso, M. D., Berndt, T., Petaja, T., Wahner,
27 A., Kerminen, V.-M., Kulmala, M., Worsnop, D. R., Wildt, J., and Mentel, T. F.: A large source
28 of low-volatility secondary organic aerosol, *Nature*, 506, 476-479, 10.1038/nature13032, 2014.

29 Emanuelsson, E. U., Watne, A. K., Lutz, A., Ljungstrom, E., and Hallquist, M.: Influence of
30 Humidity, Temperature, and Radicals on the Formation and Thermal Properties of Secondary
31 Organic Aerosol (SOA) from Ozonolysis of beta-Pinene, *J. Phys. Chem. A*, 117, 10346-10358,
32 10.1021/jp4010218, 2013.

33 Epstein, S. A., Riipinen, I., and Donahue, N. M.: A Semiempirical Correlation between Enthalpy
34 of Vaporization and Saturation Concentration for Organic Aerosol, *Environmental Science &*
35 *Technology*, 44, 743-748, 10.1021/es902497z, 2010.

36 Fuentes, E., and McFiggans, G.: A modeling approach to evaluate the uncertainty in estimating
37 the evaporation behaviour and volatility of organic aerosols, *Atmospheric Measurement*
38 *Techniques*, 5, 735-757, 10.5194/amt-5-735-2012, 2012.

39 Gao, S., Keywood, M., Ng, N. L., Surratt, J., Varutbangkul, V., Bahreini, R., Flagan, R. C., and
40 Seinfeld, J. H.: Low-molecular-weight and oligomeric components in secondary organic aerosol
41 from the ozonolysis of cycloalkenes and alpha-pinene, *J. Phys. Chem. A*, 108, 10147-10164,
42 10.1021/jp047466e, 2004a.

43 Gao, S., Ng, N. L., Keywood, M., Varutbangkul, V., Bahreini, R., Nenes, A., He, J. W., Yoo, K.
44 Y., Beauchamp, J. L., Hodyss, R. P., Flagan, R. C., and Seinfeld, J. H.: Particle phase acidity and
45 oligomer formation in secondary organic aerosol, *Environmental Science & Technology*, 38,
46 6582-6589, 10.1021/es049125k, 2004b.

1 Grieshop, A. P., Donahue, N. M., and Robinson, A. L.: Is the gas-particle partitioning in alpha-
2 pinene secondary organic aerosol reversible?, *Geophysical Research Letters*, 34, L14810
3 10.1029/2007gl029987, 2007.

4 Guenther, A., Hewitt, C. N., Erickson, D., Fall, R., Geron, C., Graedel, T., Harley, P., Klinger, L.,
5 Lerda, M., McKay, W. A., Pierce, T., Scholes, B., Steinbrecher, R., Tallamraju, R., Taylor, J.,
6 and Zimmerman, P.: A Global-Model of Natural Volatile Organic-Compound Emissions, *J.*
7 *Geophys. Res.-Atmos.*, 100, 8873-8892, 10.1029/94jd02950, 1995.

8 Hall, W. A., and Johnston, M. V.: Oligomer Formation Pathways in Secondary Organic Aerosol
9 from MS and MS/MS Measurements with High Mass Accuracy and Resolving Power, *J. Am. Soc.*
10 *Mass Spectrom.*, 23, 1097-1108, 10.1007/s13361-012-0362-6, 2012a.

11 Hall, W. A., and Johnston, M. V.: The Thermal-Stability of Oligomers in Alpha-Pinene Secondary
12 Organic Aerosol, *Aerosol Science and Technology*, 46, 983-989, 10.1080/02786826.2012.685114,
13 2012b.

14 Hallquist, M., Wenger, J. C., Baltensperger, U., Rudich, Y., Simpson, D., Claeys, M., Dommen,
15 J., Donahue, N. M., George, C., Goldstein, A. H., Hamilton, J. F., Herrmann, H., Hoffmann, T.,
16 Iinuma, Y., Jang, M., Jenkin, M. E., Jimenez, J. L., Kiendler-Scharr, A., Maenhaut, W.,
17 McFiggans, G., Mentel, T. F., Monod, A., Prevot, A. S. H., Seinfeld, J. H., Surratt, J. D.,
18 Szmigielski, R., and Wildt, J.: The formation, properties and impact of secondary organic aerosol:
19 current and emerging issues, *Atmospheric Chemistry and Physics*, 9, 5155-5236, 2009.

20 Han, Y. M., Iwamoto, Y., Nakayama, T., Kawamura, K., and Mochida, M.: Formation and
21 evolution of biogenic secondary organic aerosol over a forest site in Japan, *J. Geophys. Res.-*
22 *Atmos.*, 119, 259-273, 10.1002/2013jd020390, 2014.

23 Henry, K. M., Lohaus, T., and Donahue, N. M.: Organic Aerosol Yields from alpha-Pinene
24 Oxidation: Bridging the Gap between First-Generation Yields and Aging Chemistry,
25 *Environmental Science & Technology*, 46, 12347-12354, 10.1021/es302060y, 2012.

26 Huffman, J. A., Ziemann, P. J., Jayne, J. T., Worsnop, D. R., and Jimenez, J. L.: Development and
27 characterization of a fast-stepping/scanning thermodenuder for chemically-resolved aerosol
28 volatility measurements, *Aerosol Science and Technology*, 42, 395-407,
29 10.1080/02786820802104981, 2008.

30 Kalberer, M., Paulsen, D., Sax, M., Steinbacher, M., Dommen, J., Prevot, A. S. H., Fisseha, R.,
31 Weingartner, E., Frankevich, V., Zenobi, R., and Baltensperger, U.: Identification of polymers as
32 major components of atmospheric organic aerosols, *Science*, 303, 1659-1662,
33 10.1126/science.1092185, 2004.

34 Kannosto, J., Yli-Pirila, P., Hao, L. Q., Leskinen, J., Jokiniemi, J., Makela, J. M., Joutsensaari, J.,
35 Laaksonen, A., Worsnop, D. R., Keskinen, J., and Virtanen, A.: Bounce characteristics of alpha-
36 pinene-derived SOA particles with implications to physical phase, *Boreal Environment Research*,
37 18, 329-340, 2013.

38 Karnezi, E., Riipinen, I., and Pandis, S. N.: Measuring the atmospheric organic aerosol volatility
39 distribution: a theoretical analysis, *Atmos. Meas. Tech.*, 2953-2965, 10.5194/amt-7-2953-2014,
40 2014.

41 Kesselmeier, J., and Staudt, M.: Biogenic volatile organic compounds (VOC): An overview on
42 emission, physiology and ecology, *Journal of Atmospheric Chemistry*, 33, 23-88,
43 10.1023/a:1006127516791, 1999.

44 Koop, T., Bookhold, J., Shiraiwa, M., and Poschl, U.: Glass transition and phase state of organic
45 compounds: Dependency on molecular properties and implications for secondary organic aerosols

1 in the atmosphere, *Physical Chemistry Chemical Physics*, 13, 19238-19255, 10.1039/c1cp22617g,
2 2011.

3 Kostenidou, E., Lee, B. H., Engelhart, G. J., Pierce, J. R., and Pandis, S. N.: Mass Spectra
4 Deconvolution of Low, Medium, and High Volatility Biogenic Secondary Organic Aerosol,
5 *Environmental Science & Technology*, 43, 4884-4889, 10.1021/es803676g, 2009.

6 Kourtchev, I., Fuller, S. J., Giorio, C., Healy, R. M., Wilson, E., O'Connor, I., Wenger, J. C.,
7 McLeod, M., Aalto, J., Ruuskanen, T. M., Maenhaut, W., Jones, R., Venables, D. S., Sodeau, J.
8 R., Kulmala, M., and Kalberer, M.: Molecular composition of biogenic secondary organic aerosols
9 using ultrahigh-resolution mass spectrometry: comparing laboratory and field studies,
10 *Atmospheric Chemistry and Physics*, 14, 2155-2167, 10.5194/acp-14-2155-2014, 2014.

11 Kristensen, K., Enggrob, K. L., King, S. M., Worton, D. R., Platt, S. M., Mortensen, R., Rosenoern,
12 T., Surratt, J. D., Bilde, M., Goldstein, A. H., and Glasius, M.: Formation and occurrence of dimer
13 esters of pinene oxidation products in atmospheric aerosols, *Atmos. Chem. Phys.*, 13, 3763-3776,
14 10.5194/acp-13-3763-2013, 2013.

15 Kristensen, K., Cui, T., Zhang, H., Gold, A., Glasius, M., and Surratt, J. D.: Dimers in alpha-pinene
16 secondary organic aerosol: effect of hydroxyl radical, ozone, relative humidity and aerosol acidity,
17 *Atmospheric Chemistry and Physics*, 14, 4201-4218, 10.5194/acp-14-4201-2014, 2014.

18 Kundu, S., Fisseha, R., Putman, A. L., Rahn, T. A., and Mazzoleni, L. R.: High molecular weight
19 SOA formation during limonene ozonolysis: insights from ultrahigh-resolution FT-ICR mass
20 spectrometry characterization, *Atmospheric Chemistry and Physics*, 12, 5523-5536, 10.5194/acp-
21 12-5523-2012, 2012.

22 Lee, B. H., Kostenidou, E., Hildebrandt, L., Riipinen, I., Engelhart, G. J., Mohr, C., DeCarlo, P.
23 F., Mihalopoulos, N., Prevot, A. S. H., Baltensperger, U., and Pandis, S. N.: Measurement of the
24 ambient organic aerosol volatility distribution: application during the Finokalia Aerosol
25 Measurement Experiment (FAME-2008), *Atmospheric Chemistry and Physics*, 10, 12149-12160,
26 10.5194/acp-10-12149-2010, 2010.

27 Lee, B. H., Pierce, J. R., Engelhart, G. J., and Pandis, S. N.: Volatility of secondary organic aerosol
28 from the ozonolysis of monoterpenes, *Atmos. Environ.*, 45, 2443-2452,
29 10.1016/j.atmosenv.2011.02.004, 2011.

30 Loza, C. L., Coggon, M. M., Nguyen, T. B., Zuend, A., Flagan, R. C., and Seinfeld, J. H.: On the
31 Mixing and Evaporation of Secondary Organic Aerosol Components, *Environmental Science &
32 Technology*, 47, 6173-6180, 10.1021/es400979k, 2013.

33 Matsunaga, A., and Ziemann, P. J.: Yields of beta-hydroxynitrates, dihydroxynitrates, and
34 trihydroxynitrates formed from OH radical-initiated reactions of 2-methyl-1-alkenes, *Proceedings
35 of the National Academy of Sciences of the United States of America*, 107, 6664-6669,
36 10.1073/pnas.0910585107, 2010.

37 Muller, L., Reinnig, M. C., Hayen, H., and Hoffmann, T.: Characterization of oligomeric
38 compounds in secondary organic aerosol using liquid chromatography coupled to electrospray
39 ionization Fourier transform ion cyclotron resonance mass spectrometry, *Rapid Communications
40 in Mass Spectrometry*, 23, 971-979, 10.1002/rcm.3957, 2009.

41 Odum, J. R., Hoffmann, T., Bowman, F., Collins, D., Flagan, R. C., and Seinfeld, J. H.:
42 Gas/particle partitioning and secondary organic aerosol yields, *Environmental Science &
43 Technology*, 30, 2580-2585, 1996.

44 Pankow, J. F.: An Absorption-Model of the Gas Aerosol Partitioning Involved in the Formation
45 of Secondary Organic Aerosol, *Atmos. Environ.*, 28, 189-193, 1994.

1 Pathak, R. K., Presto, A. A., Lane, T. E., Stanier, C. O., Donahue, N. M., and Pandis, S. N.:
2 Ozonolysis of alpha-pinene: parameterization of secondary organic aerosol mass fraction,
3 *Atmospheric Chemistry and Physics*, 7, 3811-3821, 2007.

4 Putman, A. L., Offenberg, J. H., Fisseha, R., Kundu, S., Rahn, T. A., and Mazzoleni, L. R.:
5 Ultrahigh-resolution FT-ICR mass spectrometry characterization of alpha-pinene ozonolysis SOA,
6 *Atmos. Environ.*, 46, 164-172, 10.1016/j.atmosenv.2011.10.003, 2012.

7 Riipinen, I., Pierce, J. R., Donahue, N. M., and Pandis, S. N.: Equilibration time scales of organic
8 aerosol inside thermodenuders: Evaporation kinetics versus thermodynamics, *Atmos. Environ.*,
9 44, 597-607, 10.1016/j.atmosenv.2009.11.022, 2010.

10 Roldin, P., Eriksson, A. C., Nordin, E. Z., Hermansson, E., Mogensen, D., Rusanen, A., Boy, M.,
11 Swietlicki, E., Svenningsson, B., Zelenyuk, A., and Pagels, J.: Modelling non-equilibrium
12 secondary organic aerosol formation and evaporation with the aerosol dynamics, gas- and particle-
13 phase chemistry kinetic multilayer model ADCHAM, *Atmospheric Chemistry and Physics*, 14,
14 7953-7993, 10.5194/acp-14-7953-2014, 2014.

15 Saleh, R., Shihadeh, A., and Khlystov, A.: On transport phenomena and equilibration time scales
16 in thermodenuders, *Atmospheric Measurement Techniques*, 4, 571-581, 10.5194/amt-4-571-2011,
17 2011.

18 Saleh, R., Donahue, N. M., and Robinson, A. L.: Time Scales for Gas-Particle Partitioning
19 Equilibration of Secondary Organic Aerosol Formed from Alpha-Pinene Ozonolysis,
20 *Environmental Science & Technology*, 47, 5588-5594, 10.1021/es400078d, 2013.

21 Salo, K., Hallquist, M., Jonsson, A. M., Saathoff, H., Naumann, K. H., Spindler, C., Tillmann, R.,
22 Fuchs, H., Bohn, B., Rubach, F., Mentel, T. F., Muller, L., Reinnig, M., Hoffmann, T., and
23 Donahue, N. M.: Volatility of secondary organic aerosol during OH radical induced ageing,
24 *Atmospheric Chemistry and Physics*, 11, 11055-11067, 10.5194/acp-11-11055-2011, 2011.

25 Saxena, P., and Hildemann, L. M.: Water-soluble organics in atmospheric particles: A critical
26 review of the literature and application of thermodynamics to identify candidate compounds,
27 *Journal of Atmospheric Chemistry*, 24, 57-109, 1996.

28 Seinfeld, J. H., and Pankow, J. F.: Organic atmospheric particulate material, *Annu. Rev. Phys.*
29 *Chem.*, 54, 121-140, 10.1146/annurev.physchem.54.011002.103756, 2003.

30 Shilling, J. E., Chen, Q., King, S. M., Rosenoern, T., Kroll, J. H., Worsnop, D. R., DeCarlo, P. F.,
31 Aiken, A. C., Sueper, D., Jimenez, J. L., and Martin, S. T.: Loading-dependent elemental
32 composition of alpha-pinene SOA particles, *Atmospheric Chemistry and Physics*, 9, 771-782,
33 2009.

34 Stanier, C. O., Pathak, R. K., and Pandis, S. N.: Measurements of the volatility of aerosols from
35 alpha-piniene ozonolysis, *Environmental Science & Technology*, 41, 2756-2763,
36 10.1021/es0519280, 2007.

37 Tolocka, M. P., Jang, M., Ginter, J. M., Cox, F. J., Kamens, R. M., and Johnston, M. V.: Formation
38 of oligomers in secondary organic aerosol, *Environmental Science & Technology*, 38, 1428-1434,
39 10.1021/es035030r, 2004.

40 Trump, E. R., and Donahue, N. M.: Oligomer formation within secondary organic aerosols:
41 equilibrium and dynamic considerations, *Atmospheric Chemistry and Physics*, 14, 3691-3701,
42 10.5194/acp-14-3691-2014, 2014.

43 Vaden, T. D., Imre, D., Beránek, J., Shrivastava, M., and Zelenyuk, A.: Evaporation kinetics and
44 phase of laboratory and ambient secondary organic aerosol, *Proceedings of the National Academy*
45 *of Sciences of the United States of America*, 108, 2190-2195, 10.1073/pnas.1013391108, 2011.

1 Virtanen, A., Joutsensaari, J., Koop, T., Kannosto, J., Yli-Pirila, P., Leskinen, J., Makela, J. M.,
2 Holopainen, J. K., Poschl, U., Kulmala, M., Worsnop, D. R., and Laaksonen, A.: An amorphous
3 solid state of biogenic secondary organic aerosol particles, *Nature*, 467, 824-827,
4 10.1038/nature09455, 2010.
5 Weber, R. J., Sullivan, A. P., Peltier, R. E., Russell, A., Yan, B., Zheng, M., de Gouw, J., Warneke,
6 C., Brock, C., Holloway, J. S., Atlas, E. L., and Edgerton, E.: A study of secondary organic aerosol
7 formation in the anthropogenic-influenced southeastern United States, *J. Geophys. Res.-Atmos.*,
8 112, 10.1029/2007jd008408, 2007.
9 Wilson, J., Imre, D., Beranek, J., Shrivastava, M., and Zelenyuk, A.: Evaporation Kinetics of
10 Laboratory-Generated Secondary Organic Aerosols at Elevated Relative Humidity, *Environmental*
11 *Science & Technology*, 49, 243-249, 2015.
12 Yasmeen, F., Vermeylen, R., Szmigielski, R., Iinuma, Y., Boge, O., Herrmann, H., Maenhaut, W.,
13 and Claeys, M.: Terpenylic acid and related compounds: precursors for dimers in secondary
14 organic aerosol from the ozonolysis of alpha- and beta-pinene, *Atmospheric Chemistry and*
15 *Physics*, 10, 9383-9392, 10.5194/acp-10-9383-2010, 2010.
16 Zaveri, R. A., Easter, R. C., Shilling, J. E., and Seinfeld, J. H.: Modeling kinetic partitioning of
17 secondary organic aerosol and size distribution dynamics: representing effects of volatility, phase
18 state, and particle-phase reaction, *Atmospheric Chemistry and Physics*, 14, 5153-5181,
19 10.5194/acp-14-5153-2014, 2014.
20 Zhang, Q., Worsnop, D. R., Canagaratna, M. R., and Jimenez, J. L.: Hydrocarbon-like and
21 oxygenated organic aerosols in Pittsburgh: insights into sources and processes of organic aerosols,
22 *Atmospheric Chemistry and Physics*, 5, 3289-3311, 2005.
23 Zhang, X., Cappa, C. D., Jathar, S. H., McVay, R. C., Ensberg, J. J., Kleeman, M. J., and Seinfeld,
24 J. H.: Influence of vapor wall loss in laboratory chambers on yields of secondary organic aerosol,
25 *Proceedings of the National Academy of Sciences of the United States of America*, 111, 5802-
26 5807, 10.1073/pnas.1404727111, 2014.

27

28

1 **Table 1.** Experimental conditions for α -pinene + O₃ SOA generation for the various experiments.

Experiment Date	Flowrate (lpm)	Initial C _{OA} ($\mu\text{g m}^{-3}$)	C _{OA} after dilution ($\mu\text{g m}^{-3}$)	α -pinene ($\mu\text{L hr}^{-1}$)	Ozone (ppm)	$d_{p,V,bypass}$ (nm)
90512	0.79	1	n/a	0.12	4.9	37
82912	0.8	9	n/a	0.12	7.8	39
101912	0.8	30	n/a	0.6	8.8	52
41114	0.82	90	n/a	0.15	38.7	48
90712	0.81	150	n/a	0.3	6.8	61
91312	0.8	180	n/a	0.2	^	57
40914	0.82	200	n/a	0.23*	63	57
91212	0.8	400	n/a	0.5	^	73
101612	0.8	450	n/a	0.6	8.8	83
101712	0.8	500	n/a	0.6	8.8	88
091112	0.8	600	n/a	0.38	23.4	76
101812	0.83	800	n/a	0.6	8.8	97
101212	0.83	380	5	0.6	8.8	73
100912	1.02	380	6	0.7	9.8	71
101112	0.79	430	7	0.5	9.7	73
101012	0.8	450	10	0.5	8.8	77
83112	0.8	600	14	0.5	29.3	76
92412	0.76	650	23	0.5	9.7	90
100412	1.04	450	23	0.5	8.8	68

*The flowrate of N₂ over the α -pinene syringe was 0.015 lpm for all experiments except this one, for which it was 0.074 lpm.

^ Unknown

2

3

1 **Table 2.** The average fit parameters for each C_{OA} grouping of mass thermograms.

Mass Loading Range ($\mu\text{g m}^{-3}$)	$S_{VFR} \pm \sigma_e^{\#}$	$T_{50} \pm \sigma_e$ (K)	# of Samples
Diluted (<23)	-15.9 ± 1.6	346 ± 7	7
Low (≤ 30)	-16.6 ± 1.9	345 ± 5	3
Medium ($90 < C_{OA} < 200$)	-15.7 ± 1.6	347 ± 6	4
High (>300)	-16.4 ± 1.5	359 ± 7	5

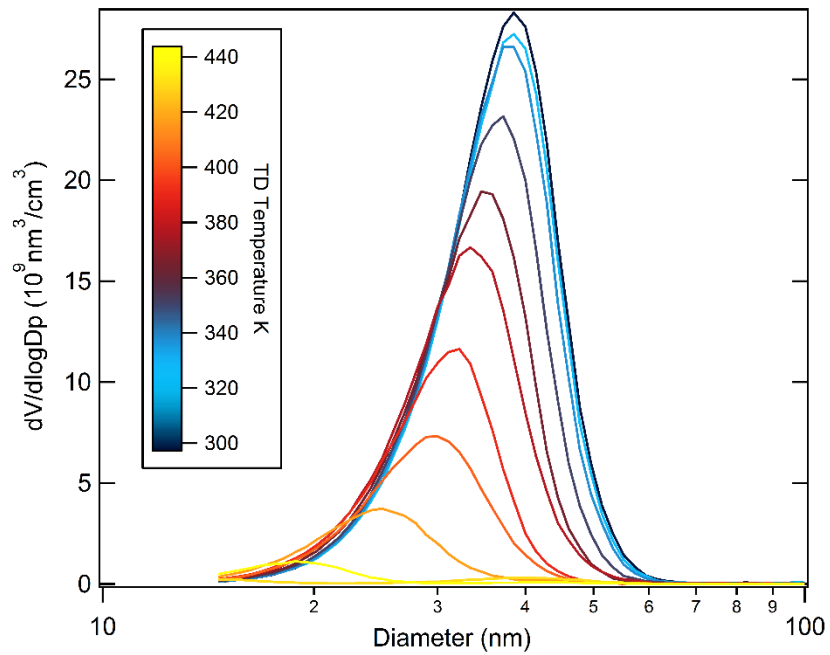
[#] σ_e is the greater of the propagation of error from the individual fits and the sample standard deviation.

2

3

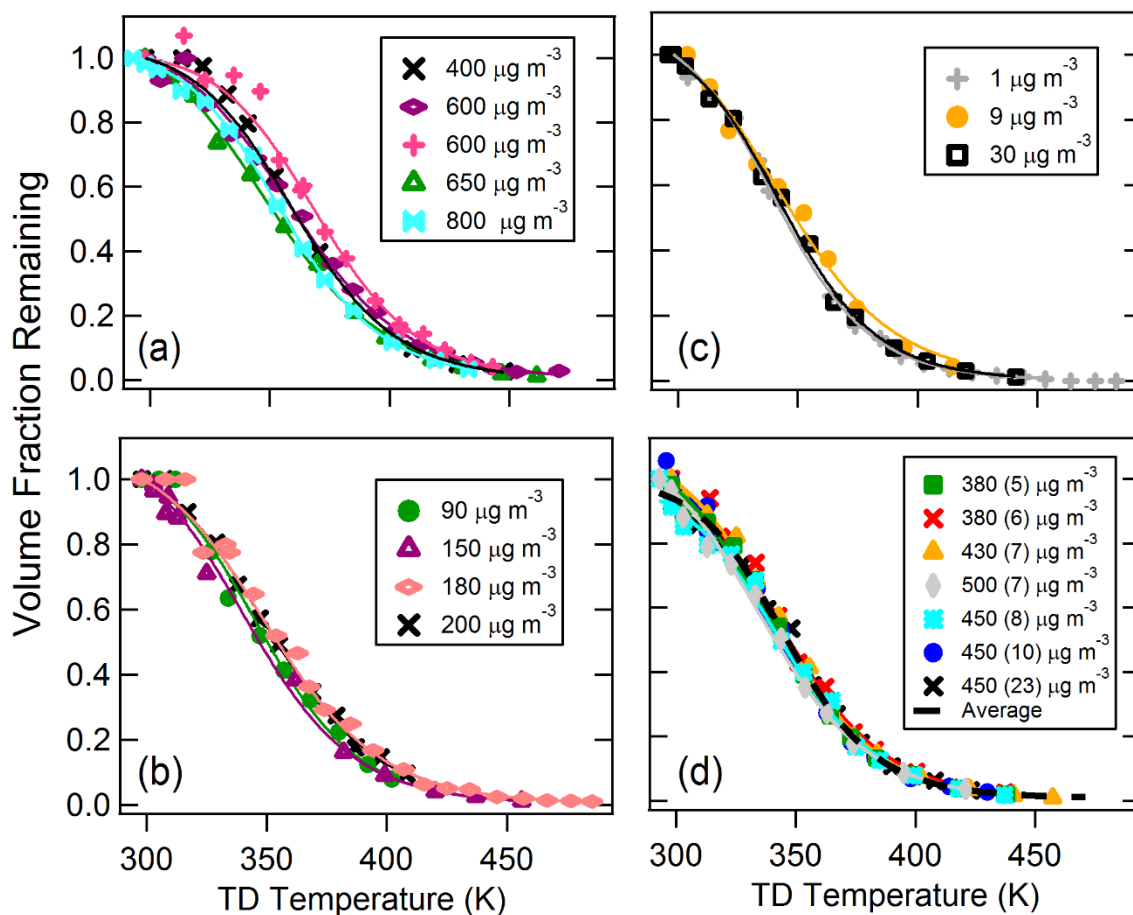
4

1
2



3
4
5
6
7

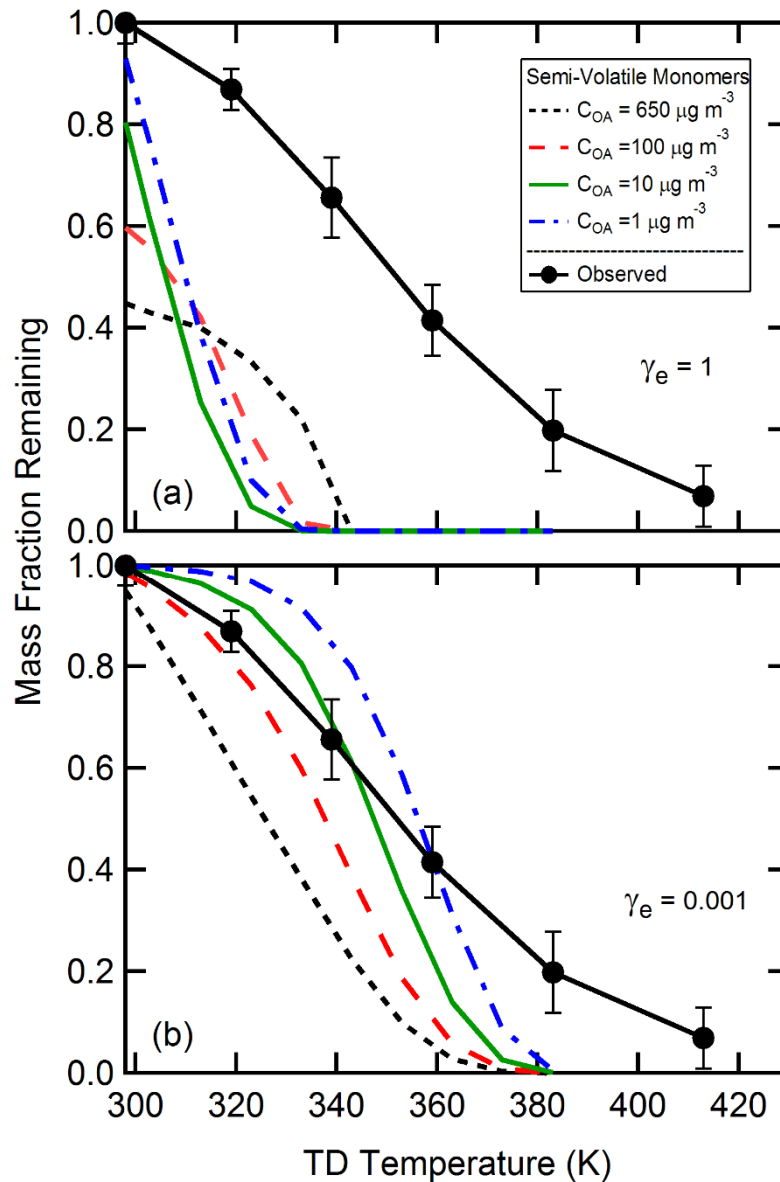
Figure 1. An example of the particle volume weighted size distributions observed as a function of TD temperature from one experiment. The temperatures range from room temperature (296 K, light blue) to 453 K (purple). This experiment had a bypass $C_{OA} = 9\mu\text{g m}^{-3}$ and $d_{p,V,bypass} = 39\text{ nm}$.



1
 2 **Figure 2.** Mass thermograms measured for each of the experiments (symbols). Results are grouped
 3 according to the bypass mass loading as (a) high ($C_{OA} > 300 \mu\text{g m}^{-3}$), (b) medium ($90 \leq C_{OA} < 300$
 4 $\mu\text{g m}^{-3}$), and (c) low loading ($C_{OA} \leq 30 \mu\text{g m}^{-3}$). Results from isothermal dilution experiments are
 5 shown in (d), where the initial number is the C_{OA} before dilution and the number in parentheses
 6 that after dilution. Traces represent the fit of Eq. 2 to each experiment.

7

1

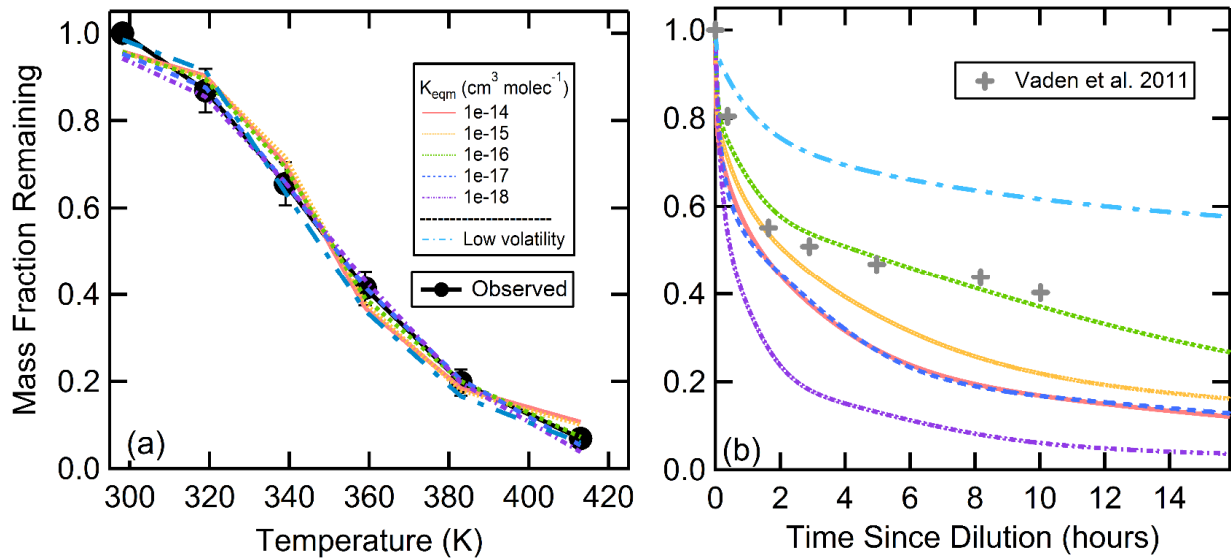


2

3 **Figure 3.** Model predictions for the mass thermograms of α -pinene+O₃ SOA using the semi-
 4 volatile monomer TD model where the initial model C_{OA} was $650 \mu\text{g m}^{-3}$ (black, short dash), 100
 5 $\mu\text{g m}^{-3}$ (red, long dash), $10 \mu\text{g m}^{-3}$ (green, solid) or $1 \mu\text{g m}^{-3}$ (blue, dot-dash) for evaporation
 6 coefficients, γ_e , equal to (a) 1 and (b) 0.001. Neither set of predictions agree well with the observed
 7 mass thermogram for medium/low C_{OA} (black line with black \bullet).

8

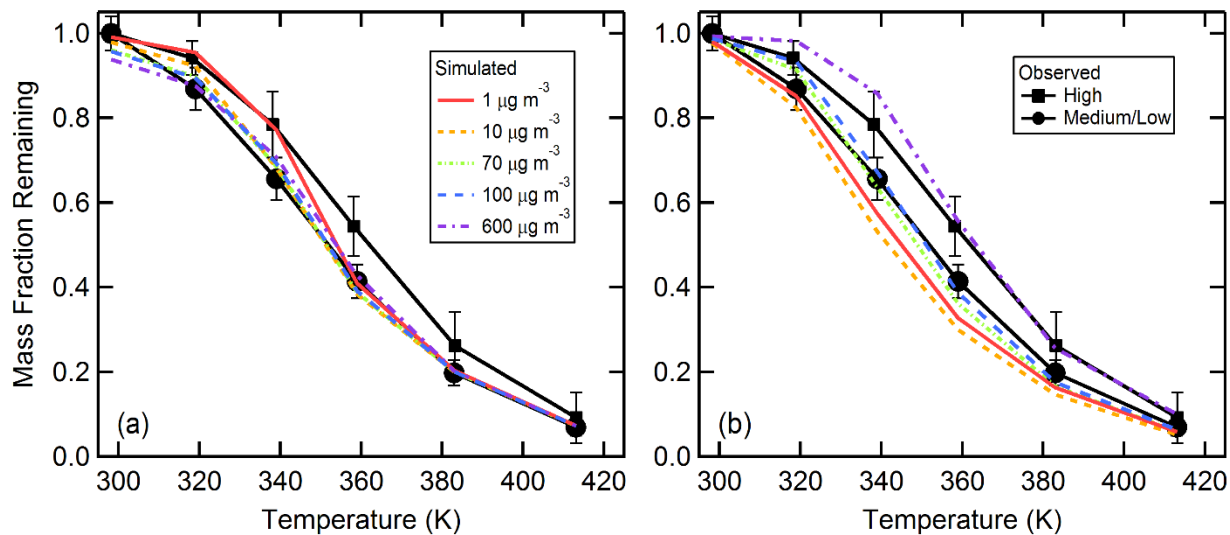
1
2



3

4 **Figure 4.** (a) Comparison between observed medium/low C_{OA} grouping (black ●) and best-fit
5 calculated mass thermograms for the TD model that includes dimer decomposition and for the
6 low-volatility compound model. For the dimer-decomposition model, the concentration of dimers
7 is much greater than the concentration of monomers. (b) Simulated isothermal, room temperature
8 evaporation based on the best-fit model parameters determined in (a). The initial SOA
9 concentration was $100 \mu\text{g m}^{-3}$, which was diluted by a factor of 30 and evaporated vapors were
10 lost to the simulated chamber walls with a rate coefficient of 10^{-3}s^{-1} . The grey crosses (+) in panel
11 b are the experimental data from the isothermal dilution of α -pinene+ O_3 SOA ($d_p = 160 \text{ nm}$) from
12 Vaden et al. (2011).

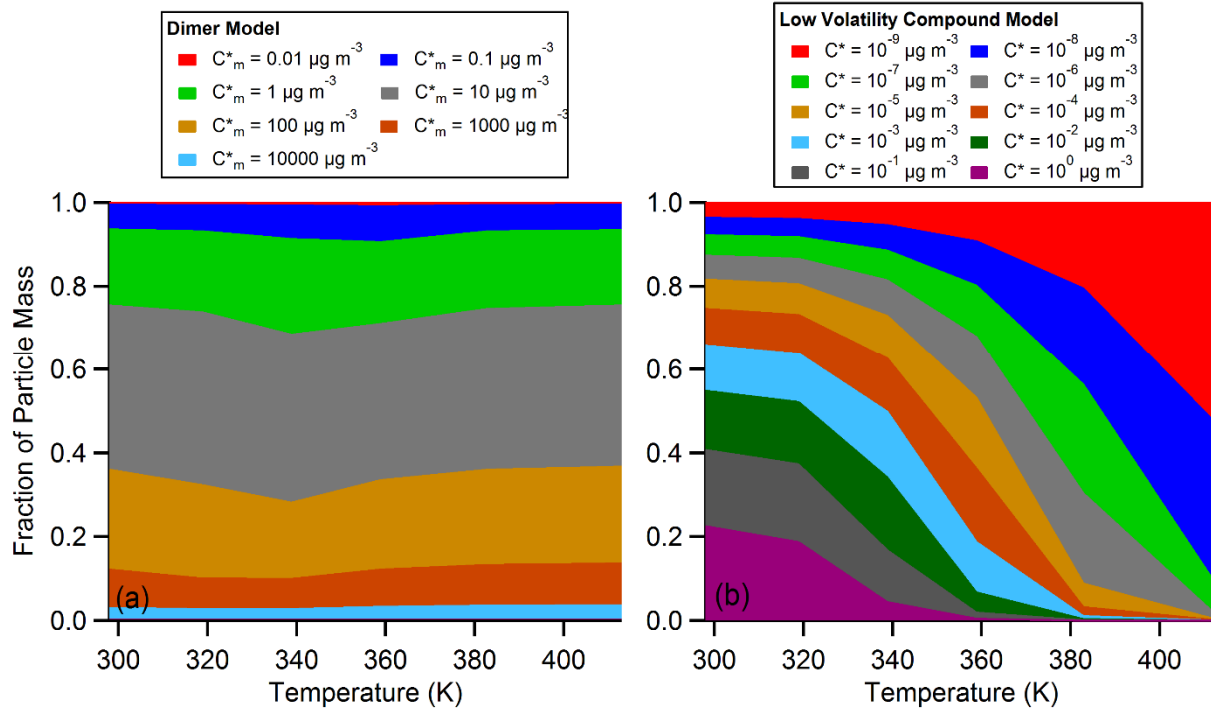
13



1
 2 **Figure 5.** (a) Calculated mass thermograms for variable C_{OA} based on the best-fit parameters for
 3 the $K_{eqm} = 10^{-16} \text{ cm}^3 \text{ molecules}^{-1}$ dimer-decomposition model as compared to the observations for
 4 the average medium/low and high C_{OA} . (b) Same as (a), but for the best-fit low-volatility model.

5
 6

1

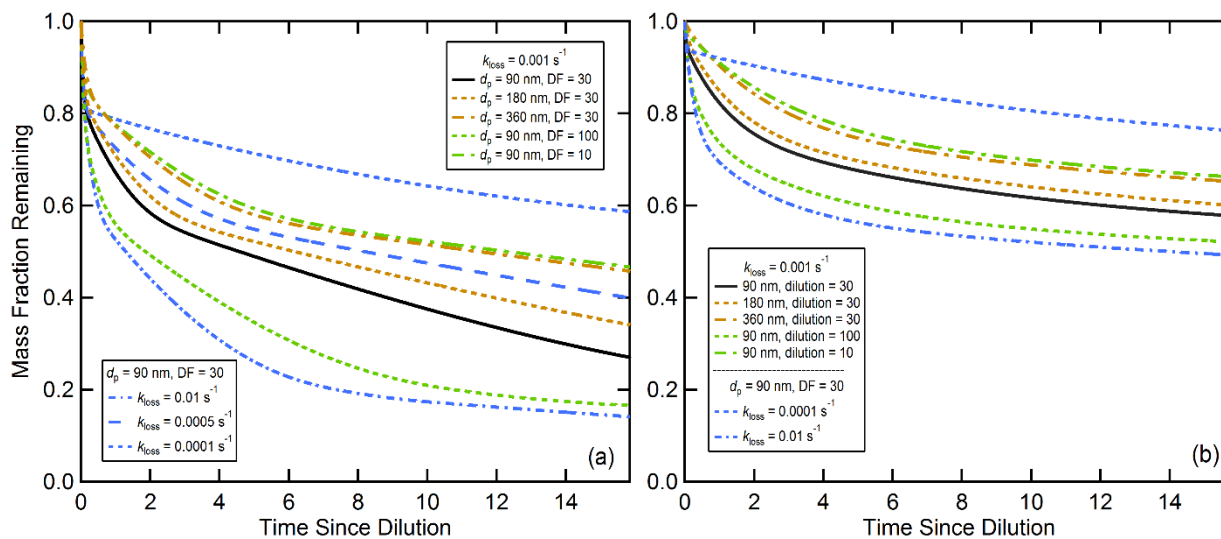


2

3 **Figure 6.** Variation in the relative particle composition with temperature from the (a) dimer-
 4 decomposition and (b) low-volatility monomer evaporation TD models. The colors correspond to
 5 the various dimer and monomer species, defined by the monomer C^* values. For the dimer-
 6 decomposition model the monomer fractional contributions are too small to be seen, and the
 7 reported C^* values in the legend correspond to the parent monomer values associated with each
 8 dimer. For the low-volatility monomer case, the C^* values correspond to the actual evaporating
 9 monomer values. The simulations were run for an initial $C_{OA} = 100 \mu\text{g m}^{-3}$.

10

1



2

3 **Figure 7.** Dependence of the isothermal evaporation simulations on the assumed vapor loss rate
 4 (k_{loss}), dilution factor (DF) or particle diameter (d_p) for (a) the dimer-decomposition and (b) the
 5 low-volatility models. All simulations were run for an initial $C_{\text{OA}} = 100 \mu\text{g m}^{-3}$. For the dimer-
 6 decomposition model, the $K_{\text{eqm}} = 10^{-16} \text{ cm}^3 \text{ molecules}^{-1}$ best-fit results were used.